PHILOSOPHICAL TRANSACTIONS OF THE ROYAL SOCIETY A

Phil. Trans. R. Soc. A (2012) **370**, 1505–1542
doi:10.1098/rsta.2011.0457

Seismically generated tsunamis

By Diego Arcas[1,2] and Harvey Segur[3,*]

[1]*NOAA Center for Tsunami Research, Pacific Marine Environmental Laboratory, National Oceanic and Atmospheric Administration, Seattle, WA 98115-6349, USA*
[2]*Joint Institute for the Study of the Atmosphere and Ocean, University of Washington, Seattle, WA 98195-5672, USA*
[3]*Department of Applied Mathematics, University of Colorado, Boulder, CO 80309-0526, USA*

People around the world know more about tsunamis than they did 10 years ago, primarily because of two events: a tsunami on 26 December 2004 that killed more than 200 000 people around the shores of the Indian Ocean; and an earthquake and tsunami off the coast of Japan on 11 March 2011 that killed nearly 15 000 more and triggered a nuclear accident, with consequences that are still unfolding. This paper has three objectives: (i) to summarize our current knowledge of the dynamics of tsunamis; (ii) to describe how that knowledge is now being used to forecast tsunamis; and (iii) to suggest some policy changes that might protect people better from the dangers of future tsunamis.

Keywords: nonlinear water waves; dynamics of tsunamis; tsunami forecasting; tsunami hazard mitigation

1. Dynamics of tsunamis

A tsunami is a wave or set of waves that carries an enormous volume of water, and that was generated by an undersea earthquake or landslide. This paper focuses primarily on tsunamis generated by undersea earthquakes, because up to 75 per cent of all recorded tsunamis were generated in this way [1].

(*a*) *The destructive power of a tsunami*

Tsunamis are important because they can be so terribly destructive to life and property. An example of the destructive power of a tsunami is visible from its effect on Kesennuma, a Japanese port that was destroyed by the tsunami of 11 March 2011. A record of that destruction as it occurs can be seen at http://www.youtube.com/watch?v=tu056xg4hc8. (The dynamics of tsunamis can be seen more easily in videos and animations than in still photos. In addition, because of the availability of audio/visual recording devices in today's world, the tsunamis of 2004 and 2011 were documented much more than any

*Author for correspondance (segur@colorado.edu).

One contribution of 13 to a Theme Issue 'Nonlinear water waves'.

previous tsunami. This easily accessible documentation is partly responsible for the increased awareness of tsunamis in the general populace. This paper refers to some relevant videos.) The brave person holding the camera was apparently standing on the rooftop of an office building near the river. Another office building stands across a parking area, and both buildings are nestled among warehouses and other structures common to ports. During the 5–6 min duration of the video, the water level rises steadily from its usual river level to the top of the second-floor windows of the nearby office building. Even so, the water surface is always spatially flat, showing the long spatial wavelength of the tsunami. The wave period of the tsunami was also long, certainly longer than 5 min. For comparison, note that 10 s wave periods are common for wind-driven ocean waves, and that a wave with a 20 s period is unusually long. Tsunamis have wavelengths and wave periods much longer than those of any other waves on the ocean's surface, except for tides. But the important practical feature of large tsunamis is their destructive power. By the end of this video, the tsunami had washed away almost the entire town that was visible 5 min earlier. The two office buildings built with reinforced concrete seem to be the only exceptions. A second video, recorded 1 day later at Kesennuma, catalogues some of the destruction: http://www.youtube.com/watch?v=sDXcyfkg95k.

(*b*) *Analysis of the 2004 tsunami*

To understand the dynamics of tsunamis, it is convenient to consider the tsunami of 26 December 2004, generated by a chain of earthquakes in the northern Indian Ocean. Figure 1 shows a map of the Indian Ocean: India and Sri Lanka are to the left, with Burma, Thailand and Malaysia on the peninsula to the right. The long island is Sumatra, and Banda Aceh is a town located on the northern tip of Sumatra.

Earthquakes that generate tsunamis occur on the boundaries of adjacent tectonic plates, moving relative to each other. In the case shown in figure 1, the India plate is slowly sliding under the Burma plate to its east (and under the Eurasian plate to its north). The chain of Nicobar and Andaman Islands marks this plate boundary, and it also separates the Bay of Bengal (deeper and west of the island chain) from the Andaman Sea (shallower and east of the islands).

The tsunami of 2004 was generated not by one earthquake, but by a sequence of quakes, beginning near the northern tip of Sumatra and progressing further and further north along the boundary of the two plates. The result, after about 10 min, was the sea surface deformation shown in figure 1: the water surface was elevated along a broad stripe to the west of the (curved) fault line, and depressed along a stripe to the east. Here are some relevant (and approximate) length scales for this figure:

Surface elevation or depression due to earthquakes:	2 m
Water depth in the Bay of Bengal (west of the fault line):	3–4 km
Water depth in the Andaman Sea (east of the fault line):	2 km
East–west width of region of elevation or depression:	100 km
North–south extent of these regions:	1000 km.

(Note: no direct measurements of the initial vertical displacement of the sea surface exist. Here we use 2 m, but estimates by Geist *et al.* [2] go as high as 10 m.)

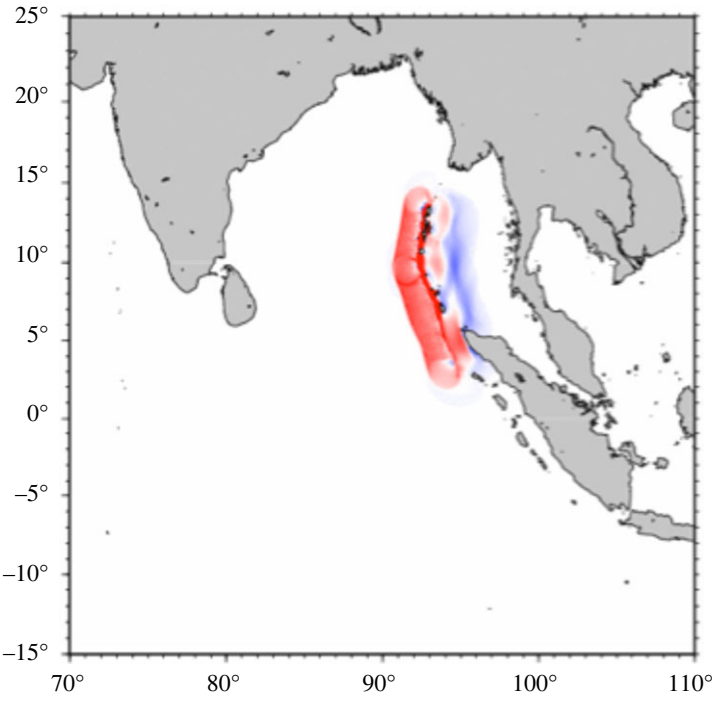

Figure 1. Map of the northern Indian Ocean, showing the shape and intensity of the initial tsunami in 2004. The coloured regions show where the water level was raised (red) and lowered (blue) by a sequence of earthquakes. This image is the first frame of a simulation of the entire tsunami by K. Satake. See http://staff.aist.go.jp/kenji.satake/animation.html for the full animation.

Mathematical models of water waves are discussed in the appendix. For this event, the important conclusions are easy to draw:

— Wave amplitudes were 1000 times smaller than the local ocean depth, so the waves that evolved from these initial data were small amplitude waves. Hence a linearized theory should describe the propagation of the waves with reasonable accuracy, at least for short times, and away from shore. (See the appendix for proper definitions of 'short time' and 'long time'. Crudely, 'short time' includes the time required for the wave to propagate some reasonable number of wavelengths of the initial disturbance. For the tsunami of 2004, this would include the time to propagate across either the Bay of Bengal (less than 15×100 km) or the Andaman Sea (less than 6×100 km).)
— Wavelengths in the east–west direction were about 30 times longer than the fluid depth for the wave propagating westward, and even more so for the wave propagating eastward. In deriving the proper mathematical model, it turns out that the square of this ratio is the relevant parameter, and the squared ratio is of the order of 1000. These were very long waves.
— For long waves of small amplitude, the speed of propagation is approximately $c = \sqrt{gd}$, where g represents gravitational acceleration and

d is the local water depth. Hence one can expect the waves to travel with speeds of about

$$\sqrt{10 \times 3500} \approx 190\,\mathrm{m\,s^{-1}} \approx 650\,\mathrm{km\,h^{-1}} \quad \text{in the Bay of Bengal,}$$
$$\sqrt{10 \times 2000} \approx 140\,\mathrm{m\,s^{-1}} \approx 500\,\mathrm{km\,h^{-1}} \quad \text{in the Andaman Sea.}$$

For comparison, the speed of a large commercial airliner is 750–800 $\mathrm{km\,h^{-1}}$, with smaller aeroplanes going slower. The tsunami that propagated towards India on 26 December 2004 had a speed comparable to that of a mid-sized commercial airliner.

(*Warning*: do not confuse the wave speed with the speed of the fluid itself; individual fluid particles attained speeds of less than 1 $\mathrm{km\,h^{-1}}$ as the wave passed. This claim is justified in the appendix.)

— As discussed in the appendix, long water waves of small amplitude, travelling in water of uniform depth, satisfy approximately the linear wave equation. Figure 1 shows that the initial data were approximately one dimension (if one ignores variations along the fault line), so a simple, crude model of the propagation of the tsunami is the wave equation in one dimension,

$$\frac{\partial^2 \eta}{\partial t^2} = c^2 \frac{\partial^2 \eta}{\partial x^2} \quad \text{and} \quad c^2 = gd, \tag{1.1}$$

where $\eta(x, t)$ is the elevation of the water surface above its mean level. If the average water depth were the same in the Bay of Bengal and in the Andaman Sea, and if the initial horizontal component of wave velocity were zero, then one solves (1.1) by sending half of the initial disturbance to the left (and normal to the wavefront in figure 1) and the other half to the right (and normal to the wavefront). In an ocean of constant depth, each of these waves then propagates without change of form. Hence, India and Sri Lanka experienced a positive wave (with the sea surface elevated), followed by a negative wave (with the sea surface depressed); the wave that went towards Thailand was the reverse: a negative wave, followed by a positive wave.

— Go to http://staff.aist.go.jp/kenji.satake/animation.html to see Satake's simulation of the 2004 tsunami. Qualitatively, it looks very much like what (1.1) predicts.

— The simulation by Satake shows that the tsunami heading west reached India after about 2 h, while the tsunami heading east reached Thailand at about the same time. The distance to Thailand is shorter, but the water in the Andaman Sea is shallower, so the eastward travelling wave moved slower, and the arrival time was about the same.

— These propagation speeds and times apply to waves that travelled hundreds of kilometres. The town of Banda Aceh, on the northern tip of Sumatra, had a very different experience. It was close to the epicentre of the first earthquake, so it felt that quake with its full force. Then that earthquake initiated a sequence of subsequent quakes, which caused more and more damage to buildings that had already been weakened. The earthquakes finally stopped after about 10 min, and the tsunami struck not long after that. Even if evacuation plans had been in place, there was no

time for a serious evacuation of the town. This is a common situation for tsunamis initiated by earthquakes that occur near a coastline: places far from the earthquake have time to evacuate before the resulting tsunami strikes; places close to the earthquake often do not have this luxury.

(*c*) *How tsunamis propagate*

The linear wave equation in one dimension, (1.1), might be the first partial differential equation to be solved completely—apparently Euler, Bernoulli and D'Alembert all worked out its general solution in about 1750 (see [3]). The solution is so simple that one might wonder how tsunamis that are described so simply could be so dangerous.

The tsunami of 2004 was unusual among tsunamis because the initial disturbance was spread over such a long fault line, as shown in figure 1. In other cases, the initial data are more localized in space, and one loses the approximately one-dimensional nature of the initial data. But small amplitude waves with very long wavelengths are common features for tsunamis. In the appendix, we derive the *shallow water equations*, (A 4*c–e*), as an approximate model of propagation of long waves. If we also linearize those equations (because tsunamis have small amplitudes away from shore), then we obtain the linear wave equation in two dimensions,

$$\frac{\partial^2\eta}{\partial t^2} = \frac{\partial}{\partial x}\left(gd(x,y)\frac{\partial\eta}{\partial x}\right) + \frac{\partial}{\partial y}\left(gd(x,y)\frac{\partial\eta}{\partial y}\right) \tag{1.2}$$

with variable speed, $c = \sqrt{gd(x,y)}$. This equation is more complicated than (1.1), but it is still simple enough to raise the question: How can tsunamis that are described so simply be so dangerous?

To answer this question, consider what would have happened to someone in a fishing boat in the middle of the Bay of Bengal on 26 December 2004. As this person fishes, a wave is rapidly approaching the boat. The wave is 1 m high, 100 km long in the direction of propagation, and 1000 km long in the transverse direction. This is an enormous amount of water, and the wave is approaching the boat at $\sqrt{gd} = 650\,\mathrm{km\,h^{-1}}$. However, the wave is 100 km long, so it takes about 9 min for the entire wave to pass the boat. So over a 9 min interval, the boat rises by about 1 m, and then it descends by 1m. In addition, the boat would feel a slight current during this time, so the boat might drift a few metres to the west over 9 min. Most people in such a boat would not even notice that the wave had gone by: in the open ocean, tsunamis are not at all dangerous.

When the wave approaches shore, everything changes. The speed of propagation is still $\sqrt{gd}$, but $d(x,y)$ decreases as the water gets shallower, so the wave slows down. More precisely, the front of the wave slows down—the back of the wave is still 100 km out at sea, so it is not slowing down. The consequence is that this very long wave compresses horizontally as the front of the wave enters more and more shallow water. But water is nearly incompressible, so if the wave compresses horizontally, it must grow vertically. The final result is that this wave, which was so small and so long that it was barely noticeable in the open ocean, becomes larger in amplitude and shorter in wavelength in shallower water, and the two assumptions that led to the linear wave equation as an approximate model in the open ocean both break down near shore. The dynamics of the tsunami,

which are simple away from shore, become quite complicated near shore. Effects that can become important near shore include variations in local topography, nonlinearity, wave reflection, dispersion, breaking, vorticity and possibly more.

The most destructive part of a tsunami occurs during *inundation*, when the tsunami propagates over what had been dry land. The dynamics of a tsunami near shore are complicated, but the dynamics during inundation are even worse. Some discussion of current methods to model inundation are sketched in §2*c*, but we regard the proper mathematical modelling of a tsunami during inundation as an open question.

(*d*) *Tsunamis with soliton dynamics?*

As discussed earlier, the tsunami of 2004 had amplitudes much smaller than the fluid depth (1 m/3000 m) and wavelengths much longer than the fluid depth (100 km/3 km). In addition, the initial data were approximately one dimension, so an approximate governing equation was (1.1), at least for short times. But Korteweg & de Vries (KdV) [4] derived their now famous equation,

$$\frac{\partial F}{\partial \tau} + F\frac{\partial F}{\partial \chi} + \frac{\partial^3 F}{\partial \chi^3} = 0,$$

to describe approximately the evolution of long waves of small-to-moderate amplitude as they propagate primarily in one direction in shallow water. The KdV equation has remarkable mathematical structure, including solitons, infinitely many conservation laws, and more (see [5]). Can KdV dynamics describe tsunami evolution?

This question was considered by Pelinovsky [6], Craig [7], Segur [8], Constantin & Johnson [9], Grue *et al.* [10] and Madsen *et al.* [11]. The answer is usually 'no', as we discuss next. The small parameter (call it ε) used to derive the KdV equation is the bigger of either (wave amplitude/fluid depth) or ((fluid depth/wavelength)^2). For the tsunami of 2004, both of these numbers are about 1/1000. As discussed in the appendix, for an ocean of uniform depth, this scaling leads to the wave equation on a short time scale, during which the wave propagates over a short distance, e.g. a fixed number of wavelengths. Then the KdV equation arises on a longer time scale, during which the wave propagates over a longer distance,

$$D \sim \left(\frac{1}{\varepsilon}\right)(\text{wavelength}). \tag{1.3}$$

The initial wavelength of the 2004 tsunami was about 100 km, so the propagation distance required in order to see KdV dynamics is of the order of 1000 wavelengths, i.e. 100 000 km—much longer than the 40 000 km circumference of the Earth. Hence the 2004 tsunami could not travel far enough on Earth for KdV dynamics to become relevant. In most situations, this is the correct conclusion.

Grue *et al.* [10] discuss what might be an interesting counter-example. For the tsunami that travelled directly across the Andaman Sea, the total propagation distance to Thailand was not long enough for KdV dynamics to appear, as discussed earlier. However, part of that wave diffracted around the tip of Sumatra, and then propagated into the narrow, relatively shallow Malacca Strait (between Sumatra and Malaysia). Here the wave slowed down, so the wave amplitude

increased, and the local small parameter (ε) increased. Grue *et al.* [10] argue that the part of the tsunami that propagated along this path had enough distance for KdV dynamics to appear. However, the variable topography along this path required that the authors generalize the KdV equation to one with variable coefficients. But even this was not enough, so they used even more complicated models for their simulations.

Isolated features of the KdV model, like solitary waves and undular bores, can appear in tsunami data, and these concepts can be useful in interpreting field data. But one should be wary of expecting weakly nonlinear, weakly dispersive models like KdV (or Boussinesq, Benjamin–Bona–Mahony (BBM), etc.) to predict tsunami evolution in a quantitatively accurate way.

(See the appendix for a more complete review of approximate models of waves in shallow water.)

(*e*) *Wave dispersion*

As discussed in §2, many operational models of tsunamis use the shallow water equations, (A 4*c*–*e*), to forecast tsunamis. For long waves of very small amplitude, these equations are nearly equivalent to (1.2), so there is little difference between the two models for tsunamis far from shore. But wave amplitudes grow as a tsunami moves into shallower water, so (1.2) eventually loses its validity near shore, while the shallow water equations can handle waves of larger amplitude. But the shallow water equations are nonlinear and hyperbolic, so they also run into problems near shore—their solutions can become discontinuous in finite time, in a process called 'wave-breaking' or 'shock formation'. When that happens, one needs a rule to propagate the discontinuous functions, because the partial derivatives in (A 4*c*–*e*) have no meaning at a discontinuity. The rule needs a mathematical formulation to be useful, but the important issue is physical: Which physical process(es), omitted in the derivation of (A 4*c*–*e*), should be added to that model in order to make its discontinuous solutions physically meaningful?

This issue arises in many physical contexts, and there is no single, universal answer. Historically, the most common answer has been to include either dissipation or entropy production. (These two concepts are not identical, but are related.) Either of these leads to classical shock waves, analysed in detail in the monograph by Lax [12]. A different answer is to include wave dispersion, discussed in the appendix. Dispersive shocks occur in rarefied plasmas [13] or in Bose–Einstein condensates [14], and they are closely related to hydrodynamic undular bores [10]. Both kinds of shocks are consistent with (A 4*c*–*e*). In a classical shock, the flow variables change monotonically from one equilibrium level to another across a thin layer, while a dispersive shock is somewhat thicker, and the change from one level to another is oscillatory. The important questions for tsunami modelling are how accurately each of these models describes the shape of a breaking tsunami.

In the 1970s, J. L. Hammack carried out a series of laboratory experiments designed to model the generation and propagation of tsunamis (see [15–17]). The experiments were performed in a long wave tank, with a vertically moving piston that spanned the tank width built into the floor of the tank at one end. The length of the piston along the tank (122 cm) was much longer than the water depth (10 cm), so the waves created were always long in the sense described in

the appendix. By moving the piston up or down, Hammack generated waves of elevation or depression, respectively, and these waves then propagated to the other end of the tank. The speed of propagation was always close to $\sqrt{gd}$, where d is the depth of the quiescent water in the tank. After the waves left the generation region, they were measured as they propagated past five sequential locations down the tank. Therefore, a time-like variable in each experiment was distance down the tank, and $\{x - \sqrt{gd} \cdot t\}$ was a space-like variable.

The results of two sets of Hammack's experiments are shown in figures 2 and 3. Each set of five wave traces shows how an initially long wave of depression evolves as it propagates in shallow water of uniform depth. In each wave trace, the front of the wave is to the left, and the waves are recorded in a coordinate system moving with speed $\sqrt{gd}$. In the experiments shown, the piston was pulled down rapidly, so the initial wave shape (in the top wave trace in each set) was approximately rectangular. Because of wave reflection at the near endwall, the height of the rectangular wave was half the stroke of the piston, and the length of the rectangular wave was twice the horizontal length of the piston, as required by (1.1). The two experiments were identical, except that the stroke of the piston in figure 3 was three times larger than that in figure 2. The two waves evolved in a qualitatively similar way.

— As each wave evolved (as shown in successive wave traces down each figure), waves with shorter wavelengths receded to the rear of the wave train, because their group velocities were smaller than $\sqrt{gd}$. The front of the wave train corresponded to the longest waves, near $k = 0$. This region developed a characteristically triangular shape, and the area of this evolving triangle was approximately the area of the initial rectangle, as required by mass conservation. (This correspondence is only approximate because a small amount of the initial mass was carried in the oscillatory wave train.)
— In the solution of the linearized equations of water waves, the front of the wave is described by an Airy function, which has some similarity to the triangular region observed in the experiments. But Hammack & Segur [17] showed that predictions of the linearized equations are quantitatively quite inaccurate in the triangular-shaped region. Wave dynamics there is intrinsically nonlinear.
— The back end of the triangular region in each set of experiments is a steep wave, which marks the beginning of the 'shock'. In these two sets of experiments, this steep wave is the beginning of an oscillatory wave train, so these are dispersive shocks (or undular bores, or collisionless shocks).
— The classical water wave equations, (A 1) or (A 2), have no dissipation, but the experiments shown in figures 2 and 3 had measurable dissipation. Even so, the shocks shown in the figures are dispersive shocks, with the dissipation providing only small corrections.
— The oscillatory wave train in figure 3 clearly has much more energy in short wavelengths than that in figure 2. But the two wave trains evolved from initial data that were identical except for their wave amplitudes. So the extra energy at short wavelengths in figure 3 was generated by the dynamics of the waves as they evolved. More nonlinear interactions leads to more dispersion.

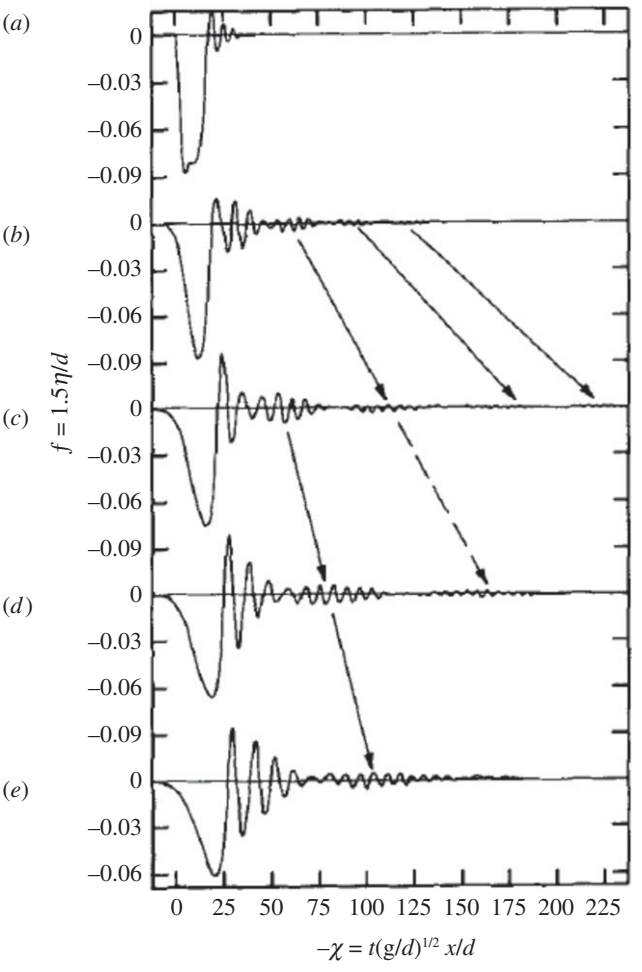

Figure 2. A long wave of depression evolves in shallow water of uniform depth (10 cm). The wavefront is to the left in each wave trace. The distance between successive wave traces is 50 depths.

The laboratory experiments shown in figures 2 and 3 show clearly that a long depression of the water surface (i.e. with the initial surface elevation below the still water level) evolves into a triangular-shaped region, carrying the negative volume of the initial wave shape, followed by a dispersive shock (which one could interpret instead to be an undular bore or an oscillatory wave train).

But what happens to an actual tsunami that is generated by a sudden depression of the sea surface? Recall from figure 1, and the animation of the 2004 tsunami, that the wave that propagated towards Thailand was in the form of a wave of depression, followed by a wave of elevation. How did the leading wave of depression evolve as it approached the shores of Thailand?

Figure 4 shows a photo of the 2004 tsunami as it hit the western shore of an island off the coast of Thailand. A photo can provide a qualitative impression, but if the photo has more than one interpretation, then there is often no good

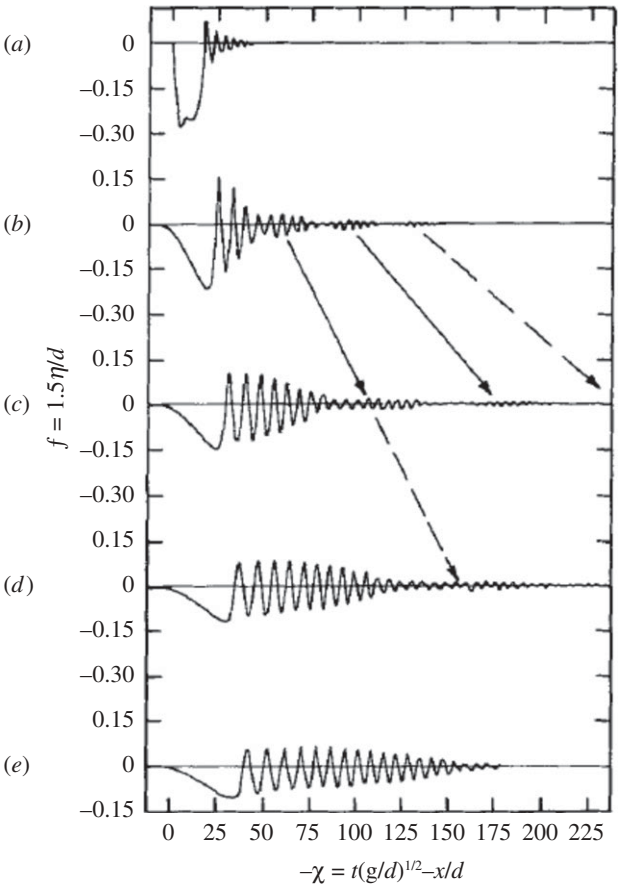

Figure 3. Same as in figure 2, except that the initial wave amplitude was three times larger than that in figure 2. Adapted from Hammack & Segur [17].

way to decide which interpretation is correct because the 'experiment' cannot be repeated. With that warning, what follows is an interpretation of the wave pattern shown in figure 4 as an oceanic example of the kind of wave pattern shown in figures 2 and 3.

Start at the lower right of the photo. The strip of light-coloured sand next to the vegetation is the usual beach, and the dark sand next to it is dark because it is normally underwater, and so temporarily waterlogged. The leading edge of the tsunami is *not* the breaking wave (marked by white foam) that begins the oscillatory wave train. This tsunami is a wave of depression: its leading edge has already reached shore, and it is sucking the normally shallow water out to sea. In figure 4, the entire region between the outer edge of the light-coloured (dry) sand and the breaking, oscillatory wave corresponds to the triangular-shaped regions in figures 2 and 3. Consider next the oscillatory wave train, behind the single breaking wave. This wave train (or undular bore, or dispersive shock) takes time to develop; at early times the first wave crest is noticeably larger than the crests that follow it. This feature is evident throughout figure 2, and at the early

Figure 4. Photo of the tsunami of 26 December 2004, hitting North Beach of Koh Jum, off the coast of Thailand. The photo was taken from the top of Mt Pu, on the island. Copyright by Anders Grawin, 2006.

times in figure 3. If the first wave crest in the wave train shown in figure 4 were larger than the crests that follow it, that would explain why only the first crest is breaking in figure 4. Constantin & Johnson [9] show a pair of photos taken on a different beach—in those photos the first two wave crests are breaking (and the crests following the first two are not visible).

Thus, the hypothesis that the wave pattern shown in figure 4 is the same kind as those in figures 2 and 3 is consistent with the information shown in the photo. If more data were available, what other features of the wave pattern would follow from this identification?

— The water ahead of the breaking wave would not have been quiescent—it was being sucked out to sea. If velocity meters had been positioned in this region, they would have shown that all of the water in this region was moving seaward. In fact, the water would have been accelerating seaward, so the water just ahead of the breaking wave would have been moving seaward faster than the water closer to shore.
— The water surface in this region ahead of the oscillatory wave train would have been fairly flat, but not horizontal. Instead the surface would have sloped slightly downhill as one goes away from shore. This downward slope is clearly evident in figures 2 and 3, but the horizontal and vertical scales on those figures were chosen to show the slope clearly. It is harder to see this on an actual water surface.

Aside from figure 4, recall the newspaper reports of the enormous loss of life from the 2004 tsunami. A common story from Thailand was the following. After the earthquakes on 26 December 2004 finally stopped, the next unusual event was

that the sea level dropped below the lowest level in anyone's memory. In many small communities along the coast of Thailand, people walked onto ground that had always been underwater, within anyone's memory, to explore the newly exposed land. Then thousands of people were killed when an enormous wave swept in. Some locations experienced one very large wave, but in other places two or three large waves were reported. If the wave pattern in figure 2 represents what happened, then all of these reports might have been correct: how many very large waves swept in might have depended on how far the evolution of the wave pattern had progressed by the time it reached shore at each location.

To summarize, both laboratory experiments and field observations indicate that dispersion plays an important role in the evolution of long waves of depression, especially near the beginning of the shock, where strong nonlinear interactions lead to additional local dispersion. Shuto [18] proposed a numerical method to approximate this dispersion while retaining the conceptual simplicity of models like (A 4*c*–*e*), by using numerical dispersion to mimic physical dispersion by the appropriate selection of time and space steps in the numerical algorithm. Burwell *et al.* [19] successfully applied this approach to a non-dispersive model in an ocean of varying depth. Their results show good correlation with analytical solutions, but the validity of this approach beyond the linear wave regime is untested, and figures 2 and 3 show that a highly nonlinear regime is precisely where physical dispersion is most important. We regard the validity of Shuto's approach for a nonlinear wave as an open question.

(*f*) *Tsunami generation*

Tsunami generation is the final topic in this discussion of the dynamics of tsunamis, but it occurs at the start of an actual tsunami. Once a tsunami has been generated at a particular location, the time required for the wave to propagate from that location to any other point in the open ocean follows from (1.2). With an accurate map of the bathymetry of the ocean (to evaluate $d(x,y)$), it is easy to calculate the arrival time of the tsunami at any distant point with reasonable accuracy, because the arrival time requires no details of the generation process except for its time and place. But some tsunamis are deadly and some are not, and that difference depends crucially on the details of their generation. For example, consider the following pair of tsunamis, discussed by Rao [20].

— A large earthquake, with a moment magnitude of $M_w = 9.1$, occurred on 26 December 2004 on the fault line between the India and Burma plates, 250 km from Banda Aceh, near the northern end of Sumatra. (For consistency, all earthquake moment magnitudes are given according to the United States Geological Survey estimates.) The epicentre of the earthquake was underwater, and it generated a tsunami that killed more than 200 000 people around the rim of the Indian Ocean.
— Another large earthquake, with a moment magnitude of 8.7, occurred on 28 March 2005 near Nias Island on the same fault line, approximately 200 km southeast of the earlier quake. Its epicentre was underwater, and its focal depth was comparable to that of the earlier quake. This earthquake killed hundreds of people, but the resulting tsunami killed no one.

Thus, accurate information about the initial conditions of the tsunami is essential to determine how dangerous a tsunami might be. Obtaining accurate information about initial conditions quickly enough to make a useful forecast is one of the major difficulties in forecasting tsunamis.

As stated earlier, most tsunamis are caused by earthquakes, and earthquakes usually occur at the boundaries of adjacent tectonic plates. But an earthquake creates a large tsunami only if it displaces a very large amount of water. It turns out that the earthquakes most likely to create dangerous tsunamis occur at *subduction zones*, where one tectonic plate is sliding beneath an adjacent plate. For example, the tsunami of 2004 was generated in the subduction zone where the India plate is sliding beneath the Burma plate, while the tsunami of 2011 was generated in the subduction zone where the Pacific plate is sliding beneath the plate that carries Japan. Figure 5 shows a world map, marking (in red) the subduction zones that the National Oceanic and Atmospheric Administration (NOAA) of the US government regards as likely sources of tsunamis. As discussed in §2, NOAA deploys instruments in these zones to obtain information about new tsunamis as quickly as possible. NOAA is one of the 26 international governmental organizations that participate in the Tsunami Warning System in the Pacific (http://www.ess.washington.edu/tsunami/general/warning/reference.html), begun in 1968. Another system was set up for the Indian Ocean after the 2004 tsunami (http://news.bbc.co.uk/2/hi/asia-pacific/5126710.stm), and a third system was launched in 2011 for the northeast Atlantic, Mediterranean and connected seas (http://www.un.org/apps/news/story.asp?NewsID=39210&Cr=tsunami&Cr1).

The relative motion of adjacent plates in a subduction zone gives rise to earthquakes and tsunamis with characteristic shapes, shown schematically in figure 6. It turns out that most of the subduction zones identified in figure 5 have either land or shallow ocean on the one side, and deep ocean on the other side. For each sketch in figure 6, envision deep ocean to the left, and either land or shallow ocean to the right.

— In figure 6*a*, one plate slides beneath an adjacent plate until there is a location (or a set of locations, or a curve) at which the two plates get stuck, and cannot slide past each other.
— In figure 6*b*, the motion of the two plates continues, but, because one point is stuck, the subducting plate tends to drag the leading edge of the overriding plate down with it. The result is that the overriding plate must bend: its leading edge is dragged down, while a region behind that edge is pushed up (because bending the rock requires less energy than compressing it). The motion of tectonic plates is measured in $\mathrm{cm\,yr^{-1}}$, so the stress in the overriding plate can build up in this way over decades or even centuries.
— Figure 6*c* shows the moment at which the stuck point becomes unstuck, releasing within seconds the energy that had built up over decades. With this rapid release of energy, the leading edge of the overriding plate jumps up and to the left, while the region behind it, which had bulged up, drops down and also moves to the left.
— The motion of the sea floor sends a pressure wave through the water above it, which generates the tsunami. As long as the energy is released quickly,

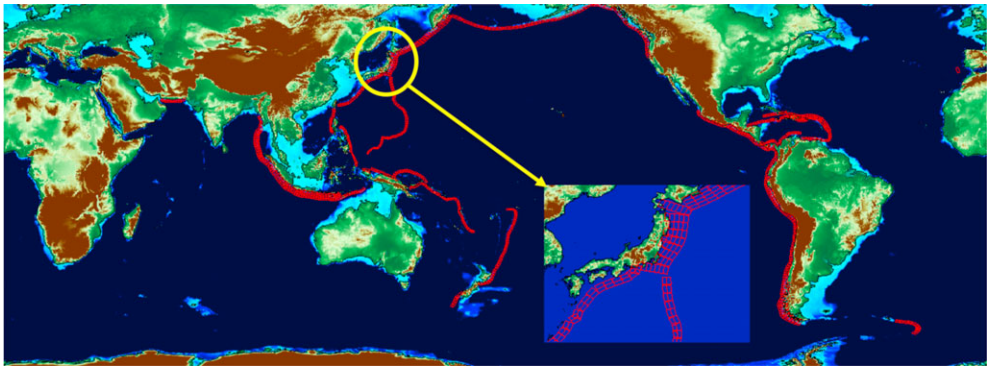

Figure 5. World map, identifying (in red) subduction zones that NOAA considers the most likely to generate tsunamis (http://nctr.pmel.noaa.gov/propagation-database.html). The insert shows details of the unit sources' extents around Japan.

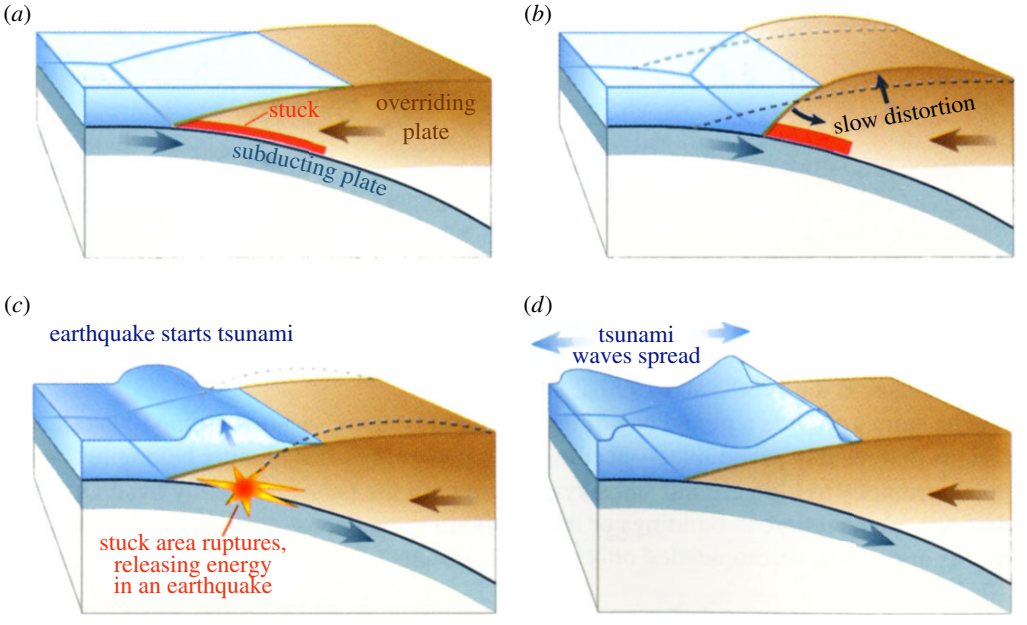

Figure 6. The relative motion of two adjacent plates in a subduction zone generates a tsunami.

then the initial shape of the free surface of the ocean copies the new shape of the ocean floor: the free surface is suddenly elevated in a region to the left (i.e. towards deeper water), while a region behind it is depressed.

Note that this schematic agrees with the inferred initial conditions for the 2004 tsunami, shown in figure 1. The Andaman Sea (to the east in figure 1) is shallower, while the Bay of Bengal is deeper. The region of elevated water level in figure 1

is to the west, towards deeper water, while the region of depressed water level is to the right, in shallower water.

The tsunami of 2011 also fits this pattern. In that case, the Pacific plate is sliding under the plate that carries Japan. The epicentre of the earthquake was only 70 km offshore, and the resulting tsunami was almost entirely a wave of elevation. The part of the Earth's crust that dropped down and to the east was mostly dry land: Japan's main island moved 2.4 m to the east (http://www.dw-world.de/dw/article/0,,14909967,00.html), and a 400 km stretch of the Japanese coast dropped 0.6 m (http://www.nytimes.com/2011/03/14/world/asia/14seismic.html?_r=1). As a result, the tsunami was devastating not only because of its size, but also because the elevation of the land had dropped.

Based on these general considerations about subduction zones, a tsunami is likely to originate in one of the marked subduction zones, like those identified in figure 5, and it is likely to have a particular shape, like that implied by figure 6. Even so, obtaining enough detailed information about the initial size and shape of a tsunami, and obtaining it quickly enough to issue a reasonably accurate forecast of the tsunami, is one of the major difficulties in forecasting tsunamis. Section 2 discusses methods currently used to obtain this information and some open questions, whose answers might lead to more accurate and/or earlier forecasts of tsunamis.

2. From tsunami warning to forecasting

Tsunamis fall into a category of natural disasters exhibiting a time scale of the order of several days from the time of tsunami generation by a seismic event to the time most of its energy has dissipated into the environment via run-up and breaking. However, the destructive stage of a tsunami typically lasts for only several hours after generation. During this period, tsunamis contain enough energy to cause major damage in coastal communities, resulting in potential loss of life and property as stated in §1. This time span of several hours, while the waves travel from the source area to the affected coastal communities in the intermediate and far fields, constrains the time window for tsunami forecasters to generate a prediction that could mitigate the impact of the waves when they make landfall on populated communities hundreds or thousands of kilometres away from the earthquake rupture area. The amount of time available to produce a forecast sets tsunamis somewhere between hurricanes for which the available forecast time is of the order of several days, and earthquakes for which no forecast is really available (and any kind of warning would have to be issued in the few minutes after or during the event at most).

In spite of the time constraints associated with tsunami forecasting, tsunami alert systems are undergoing a transition from warning to forecasting operations. Warning operations can be described as those focused on informing at-risk communities about the possibility of an impending tsunami, and forecasting operations as those intended not only to warn but also to provide estimates of the wave height, arrival time, inundation areas, currents generated and duration of the event to the population at risk. This transition has been made possible by recent scientific and technological advances, such as the increase in computational power of existing hardware and the design of deep-water tsunami sensors such

as those developed by NOAA and commonly known as Deep ocean Assessment and Reporting of Tsunamis (DART) [21,22] systems. In this section, we review some of the successes and challenges that the science of tsunami forecasting has experienced in recent years and present the most recent forecasting methodology.

Tsunamis present three clearly distinct stages to researchers concerned with forecasting their impact. We address the characteristics of each stage in §2*a–c*.

(*a*) *Tsunami generation*

The first stage of a tsunami is the *generation* stage. It lasts for approximately the duration of the rupture of the Earth's crust along the ocean bottom caused, in most cases, by a submarine earthquake. The transfer of energy from the sea floor deformation into the water column results in the deformation of the ocean surface. This deformation, driven by gravity, propagates away from the source in the form of a tsunami. As mentioned in §1, there are other geophysical phenomena in addition to seismic events that can generate long waves in the ocean, and they can also be considered tsunamis. However, we are restricting our analysis here to tsunamis of tectonic origin, that is, those generated by seismic events. It should be clarified here that we consider submarine landslides to be tsunami-generating events of seismic origin, whenever they are triggered by a seismic event and are closely associated with it in space and time. In these circumstances, they have the potential to modify the sea surface beyond what would be expected from the earthquake crustal deformation and need to be considered as part of the tsunami-generating scenario.

The main concern of a tsunami forecaster during the generation stage of a tsunami should be the identification of the ocean surface deformation that the seismic event has generated. The detection of this deformation can provide initial conditions (at least for one of the three variables present in the long wave models discussed in §1 and the appendix), which are necessary to initialize computations. These initial conditions can be grossly estimated in minutes after the earthquake based on epicentre location, earthquake magnitude and some knowledge about the geometry of the subduction zone in the rupture region. The result is a very crude approximation to the Earth-crust deformation and an even cruder estimation of ocean surface displacement. The reasons for this lack of precision in estimating initial conditions for the numerical models reside in the fact that not only epicentre location but also earthquake magnitude itself are poorly known in the instants immediately after the earthquake. We should not forget either that this is an indirect way of estimating initial conditions, i.e. this method attempts to reconstruct the sea floor deformation. It then relies on the assumption that the sea surface is deformed in an identical and simultaneous fashion to the sea floor to obtain an initial condition for tsunami models. This is not a bad assumption, at least in the linear approximation of the shallow water waves [23]. However, we are uncertain about the importance of nonlinear effects during this stage [15], as well as of the presence of other phenomena that may result in discrepancies between the sea floor and sea surface deformations, such as the presence of landslides and splay or imbricate faults, which are secondary thrust faults with very steep dip angles that can rupture simultaneously with the earthquake and result in substantial modifications to the deformation of the water surface [24].

A more accurate approach to the detection of tsunami generation is to measure directly the deformation of the sea surface as a function of time in the vicinity of the rupture area, even if only at discrete locations. This is currently possible owing to the deployment of an ocean-wide network of 51 deep-water tsunami sensors, a.k.a. DART buoys [21], by NOAA in partnership with other countries such as Chile, Australia, Indonesia, Thailand and Russia. DART buoys are essentially systems that include a bottom pressure recorder (BPR) unit deployed on the sea floor at a depth of approximately 4–5 km, and capable of measuring changes in the elevation of the ocean surface of the order of a half-centimetre [22]. The BPR sensor communicates acoustically with the surface unit, which contains the communications systems to relay the acoustic signal from the BPR to the tsunami warning centres via satellite. The DART systems sample the elevation of the ocean surface every minute during a tsunami event. With typical tsunami periods in deep water of the order of 20–30 min, the DART systems provide a well-resolved time series of tsunami amplitudes at specific locations.

The position of DART systems relative to the earthquake rupture area is crucial for the timely generation of a forecast. Proximity of the sensor to the rupture zone is a major consideration because one should try to minimize tsunami travel time from the source area to the location of the sensor in order to minimize latency time for a DART-based forecast. We identify the offshore side of a subduction zone as that on the deep-water side of the trench, in the direction of the open ocean, and the onshore side as that located between the trench and the continental platform. Tsunami travel time from the source to the sensor can be reduced by locating the DART systems slightly on the offshore side of the subduction zones where tectonic earthquakes occur. The advantage of deploying these systems offshore of the trench is twofold. The first is that the ocean depth on the offshore side of the trench is several times deeper than that on the continental shelf, normally located on the onshore side. As mentioned earlier, typical values for the ocean depth offshore of the subduction trench range between 4 and 5 km, while on the onshore side the depth varies from 0 at the shoreline to several hundreds of metres. A quick inspection of the dispersion relation (A 3) in the $\kappa d \to 0$ limit reveals that waves travel towards the DART buoy much faster than they do towards the shore, which ideally should result in the DART buoys reporting water surface data before the tsunami hits the shoreline, assuming that the source area is directly between the DART and the shoreline.

The second advantage has to do with the linear behaviour that tsunamis exhibit in deep water. We explain the important implications of this property for tsunami forecasting in more detail in §2*b*. For the time being, we just note here that if we assume the nonlinear shallow water equations as our model for tsunami propagation, and consider the one-dimensional version of (A 4*c*–*e*) with varying depth, one obtains

$$\frac{\partial u}{\partial t} + u\frac{\partial u}{\partial x} + g\frac{\partial h}{\partial x} = \frac{\partial d}{\partial x} \tag{2.1}$$

and

$$\frac{\partial h}{\partial t} + \frac{\partial (hu)}{\partial x} = 0 \tag{2.2}$$

with $h(x,t) = d(x) + \eta(x,t)$, where $d(x)$ is the ocean depth. These can easily be rewritten in characteristic form as

$$\frac{\partial p}{\partial t} + \lambda_1 \frac{\partial p}{\partial x} = g\frac{\partial d}{\partial x} \tag{2.3a}$$

and

$$\frac{\partial q}{\partial t} + \lambda_2 \frac{\partial q}{\partial x} = g\frac{\partial d}{\partial x} \tag{2.3b}$$

via the following transformation:

$$p = u + 2\sqrt{gh} \tag{2.4a}$$

and

$$q = u - 2\sqrt{gh} \tag{2.4b}$$

with

$$\lambda_{1,2} = u \pm \sqrt{gh}. \tag{2.5}$$

It now becomes obvious that the small amplitude of tsunamis in deep water warrants the approximation $\sqrt{gh} \approx \sqrt{gd}$. We have also previously mentioned that typical values of $\sqrt{gd}$ are of the order of 650 km h^{-1}, whereas those associated with flow speeds in deep water are of the order of 1 km h^{-1}. This results in the nonlinear coefficient $u \pm \sqrt{gh} \approx \sqrt{gd}$ in the deep ocean, which linearizes the nonlinear terms in (2.3*a*,*b*). By locating DART systems on the offshore side of the trench, we ensure that they provide data in the form of time series of the tsunami in deep water during its linear propagation stage.

There are additional operational and political considerations in the deployment of the deep-water BPRs, such as the stability of the sea floor at the deployment location and the convenience of conducting operations in international waters. These arguments also favour the offshore location of the DART systems.

It should also be mentioned that other technologies, in addition to deep-water BPRs, have been investigated for early detection of tsunamis. Satellite altimetry measurements and real-time global positioning systems (RTGPS) data stand out as two of the natural alternatives to deep-water BPRs.

Satellite altimetry has been used in the past to detect ocean surface deformation in the wake of tsunamigenic earthquakes such as the Sumatra 2004 event [2,25]. Measurements of sea surface elevation, with typical tsunami wavelengths obtained from satellite-mounted altimeters, seem to have a much lower signal-to-noise ratio than those associated with BPR data of the same event. This results in much longer processing periods and lower quality data than the pressure data from DART systems. In addition to the lengthy processing periods, the current sparse density of orbiting satellites with altimetry capabilities results in long delays from the time of tsunami generation until the first satellite ground track crosses the path of the propagating wave in the ocean. As a consequence of these added delays, to date, it has not been possible to issue a tsunami forecast in real time based on information from satellite altimetry, although some credible tsunami simulations have been carried out after an event.

The use of RTGPS measurements of the co-seismic crustal deformation as a means of detecting and generating initial conditions for tsunami forecast models has been proposed in the wake of recent events such as Chile 2010 and Japan 2011 in which most of the damage and loss of human life was concentrated in the near field. The main advantage of this technology is the availability of precise measurements of the deformation experienced by the Earth's crust during the seismic event almost instantly [26]. If one assumes that the ocean surface deformation is identical to that of the Earth's crust, then this technique would provide initial conditions for the hydrodynamic model. The downside of this technique comes primarily from the fact that it is an indirect measurement of the ocean surface deformation; that is, it really measures sea floor deformation not surface displacement. In doing this, it is likely to miss the effect of other phenomena mentioned earlier and concurrent with the earthquake such as landslides, which have the potential to generate substantial discrepancies between sea floor and sea surface deformation. But the largest limitation of this technique is in the development of a network of submarine GPS units offshore of the continental shelf where most of the tsunamigenic crustal deformation takes place. To our knowledge, no country has deployed this type of network, with Japan being the only country that has installed a modest number of submarine stations on the continental shelf. Preliminary efforts to use land-based RTGPS measurements to generate initial conditions for the hydrodynamic models in real time for the $M_w = 8.8$ Chile 2010 event have been unsuccessful and resulted in a substantial underestimation of the event [27].

(*b*) *Tsunami propagation*

One could consider the second stage in tsunami forecasting, the *propagation* of the wave, to begin as soon as the initial stages of the earthquake cause the ocean surface to be deformed. However, owing to the disparity between the rupture speed of the earthquake (approx. $7000\,\mathrm{km\,h^{-1}}$) and that of the hydrodynamic wave, with earthquake rupture propagating approximately 10 times faster than the tsunami in deep water, the rupture process is usually assumed to be instantaneous. This is, typically, considered to be a good assumption, even though some numerical models are starting to investigate the near-field effect of time-dependent ruptures (see also [15]).

If we neglect the time-dependency of the generation stage, we can consider the propagation phase to begin as soon as the initial ocean surface deformation has been completed. The typical ocean floor deformation has been described in §1 and usually consists of an area of uplift located on the offshore side of the trench and responsible for the generation of a positive or leading elevation wave, and an area of subsidence towards the onshore side that usually generates a negative or leading depression wave heading directly towards the near-field coastline (and with potential to generate higher run-up than a leading elevation wave; [28,29]). This initial negative wave may or may not be perceived as such by an observer located on the beach in the rupture area, because co-seismic subsidence may have extended into the continent with the shoreline experiencing similar subsidence to that of the sea level. It is undoubtedly experienced as a withdrawal of the ocean on shorelines more distant from the epicentre; such was the case along the coasts

of Thailand and Malaysia during the Sumatra tsunami event of 2004, as evidenced by the tide gauge records in Phuket, Thailand [30]. (During the tsunami of 2011 in Japan, a similar distribution of the Earth-crust deformation occurred; however, in this case, most of the subsidence took place on dry land instead of the ocean floor, as described near the end of §1.)

With tsunami forecasting in mind, we focus for the time being on this offshore, positive, deep-water travelling wave with a distinct linear behaviour. If a spatial initial condition had been obtained from the measurements explained in §2*a*, one could, in principle, attempt to compute the propagation of the wave in real time, while the tsunami is propagating from the generation region to remote coastlines in the far field. However, to proceed in this fashion is usually impractical for tsunami forecasting for two main reasons:

— Tsunami travel times are of the order of a few hours before it makes landfall on a community for which a forecast is trying to be issued. In addition to the computational time required to simulate tsunami propagation, for a forecast to be useful, it should reach the community for which it is intended well in advance of tsunami arrival, in order for emergency management agencies to determine whether mitigation measures such as advisories to the population, beach closures or evacuations are required. These constraints hamper available time to incorporate the computation of tsunami propagation in real time from the generation to the impact area. These areas can most likely benefit from a tsunami warning, but probably not from a forecast in the sense defined at the beginning of §2.
— All three techniques to detect the initial sea surface deformation described in §2*a* give temporal information at discrete locations in the rupture area. DART systems provide time series of the sea level at fixed points, satellite altimeters generate sea elevation data for points along a transect at different times, as the satellite orbits over its ground track, and GPS measurements generate initial and final information of the crust position before, after and during the earthquake. All of these instruments provide a spatially discrete distribution of the ocean surface or ocean floor deformation in real time; however, no spatially continuous deformation as needed by numerical models is available. Consequently, no initial condition is readily available to initialize the hydrodynamic models at this point, other than some crude and preliminary seismic information about the earthquake as discussed in §2*a*.

A solution can be found to both of these problems if we take advantage of the linear behaviour of tsunamis in deep water. Because the regions of the earth where tsunamigenic earthquakes occur are well identified, we can define *unit source* deformations adjacent to each other along all subduction zones with the potential for generating tsunamis [31]. Each unit source deformation can be thought of as the sea floor deformation caused by an $M_w = 7.5$ earthquake and computed via Okada's formulas [32]. Tsunami propagation in deep water from each of these unit sources can then be pre-computed and stored in a database. If an earthquake of larger magnitude and rupture extent occurs, the tsunami propagation solution of several of these unit sources can quickly and conveniently be retrieved from the

database and combined linearly to reconstruct the correct scenario. The insert in figure 5 shows how an array of tsunami unit sources is arranged to cover all tsunamigenic regions of the globe.

The use of pre-computed linear combinations of unit sources to reconstruct developing tsunami scenarios solves the problem of time-consuming propagation computations in real time; however, it gives rise to the problem of inverting DART-reported data to obtain the parameters of such linear combinations. In particular, the scaling coefficient associated with each unit source and the selection of the correct set of unit sources to represent the tsunami of interest are crucial in obtaining an accurate forecast of the event. The most common solution to this problem is the generation of a least squares approximation to a certain data window of the time series reported by the DART buoys containing the initial tsunami wave completely or partially [33]. The number of unit sources and DART buoys to be used in the inversion are among the decisions to be made by the forecaster. Once a linear combination of unit sources is found, not only is an initial condition for the deformation of the ocean surface available, but the full tsunami propagation in deep water can be generated from the propagation database in seconds.

In practice, an initial ocean-wide forecast based entirely on seismic information can be issued minutes after the earthquake. This initial forecast can then be followed by a series of updated, more accurate forecasts based on DART-reported data and generated as the waves travel over the BPRs, as additional buoys are reached by the tsunami and as more data become available. Figure 7 shows the deep-water, Pacific-wide forecast issued by the NOAA Center for Tsunami Research for the Japanese tsunami of 11 March 2011 using this methodology.

(*c*) *Impact of tsunamis on coastal regions*

The last stage in tsunami forecasting is the computation of tsunami propagation into shallow waters and its *impact on coastal communities*. Numerical simulations seem to indicate that, for most tsunamis, the waves' linear behaviour persists after the tsunami has reached the continental shelf with nonlinear effects probably appearing only at depths of a few tens of metres. This statement, of course, is valid as long as fluid velocities associated with the tsunami remain small when compared with the propagation speed of the wave $c = \sqrt{gd}$ and the waves' amplitudes remain small compared with the bottom depth.

These conditions typically hold for most tsunamis in the far field, because the magnitude of tsunami currents and amplitudes has decayed away from the source region. An example of persistent tsunami linearity in shallow waters off the coast of Honolulu, based on acoustic Doppler current profiler (ADCP) observations and measurements of the wave amplitude for the 2006 Kuril Islands tsunami ($M_w = 8.3$), is given by Arcas & Wei [34].

This, however, is not the case in the near field, where even tsunamis of moderate size can generate large amplitude waves with strong currents in shallow waters and a strongly nonlinear behaviour.

Even though linearity is likely to be preserved well into shallow waters, the compression in wavelength experienced by the tsunami as the front part of the wave moves into shallower waters and slows down while the back part is still

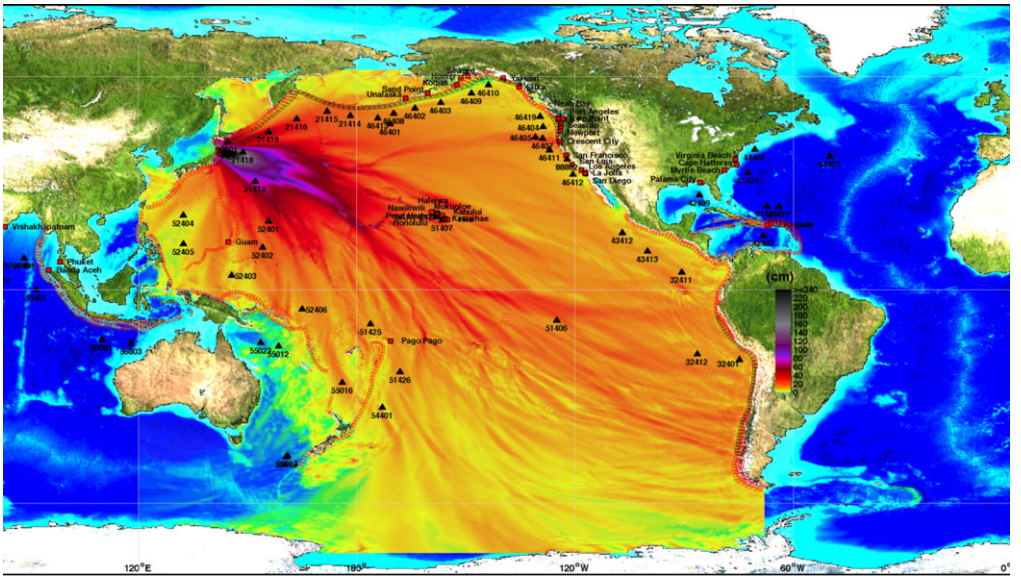

Figure 7. Distribution of the maximum amplitude of the 11 March 2011 Japanese tsunami with black triangles indicating the position of DART buoys (http://nctr.pmel.noaa.gov/database_devel.html).

in deep water and moving faster requires refinement of the computational grid used in numerical simulations. This means that real-time shallow water numerical computations should be initiated on a refined grid before the tsunami reaches the continental shelf and tsunami wavelengths become shorter. The need for grid refinement continues all the way to the shoreline as waves progressively shrink in wavelength, which means that numerical models fast enough to be used in operations have to accommodate this need by using some kind of incremental or adaptive mesh refinement so that wave dynamics at the shoreline are resolved accurately and any small features of harbours, such as jetties, breakwaters and seawalls, are well captured by the digital elevation models used to generate the bathymetric and topographic grids [35]. High-resolution grids are also crucial when the tsunami runs onto what was once dry land, because, at that stage, not only accurate representation of land structures is important but also tsunami inundation models need to incorporate a run-up algorithm that will define the new shoreline spatially at every time step. Doing this with insufficient grid resolution can result in large overestimates or underestimates of the position of the shoreline.

It is also during tsunami propagation in shallow waters and inundation that most of the tsunami energy dissipates. Because none of the physical models of tsunamis mentioned so far contain physical dissipation terms, the modeller should ensure that the run-up algorithm used in a particular model, together with the numerical dissipation inherent in it, is approximately equivalent to the physical dissipation of tsunami waves, via friction, wave-breaking and entropy generation. We have mentioned in §1*c* the complexity of the dynamics of a tsunami during inundation. The main complication arises from the need to define a moving boundary for the computational domain as the wave runs up and

down the shore. This requires the implementation of a more or less ad hoc scheme to determine the location of the waterfront that separates wet from dry land. As mentioned earlier, modelling of the water interaction with the terrain often requires the use of some energy dissipation mechanism. This is often accomplished by the use of Manning's formula for open channel flow, which requires the use of empirically determined friction coefficients associated with water flowing over different surfaces. Because, during the process of tsunami flooding, the inundating flow may encounter different types of terrain at different locations within the modelling domain, the appropriate Manning coefficient to be used would have to be spatially dependent. Furthermore, the friction properties of the dry terrain, which the first inundating wave may find, can be different from those that successive waves will encounter since they will be flowing over previously flooded terrain. This adds a temporal dependence to the optimal Manning coefficient to be used, complicating inundation modelling even further.

In addition to grid refinement, it is necessary to develop and test high-resolution tsunami forecast models for specific coastal communities for which a prediction has to be issued in the event of a tsunami [35]. These forecast models consist of grids containing the local bathymetric and topographic information necessary to compute wave evolution and inundation as the tsunami approaches coastal communities, as well as the set of numerical parameters necessary to perform the calculations. The near-shore community-specific forecast models are forced at their grid boundaries by the pre-computed, deep-water linear solution, stored in the propagation database and re-generated for a specific event via the solution to the inversion problem discussed in §2*b*.

The need for community-specific forecast models is justified for two main reasons: the large variability of tsunami run-up (defined as the difference between the elevation of the point of maximum tsunami penetration and the elevation of the shoreline at the time of tsunami arrival [36]) among nearby coastal points, and the need to maximize computational resources by focusing calculations on heavily populated areas.

Figure 8 shows values of run-up measured for the recent Japan event of 11 March 2011. The data points shown here are concentrated north of Sendai around the stretch of coast where the maximum run-up values were observed, between 35° and 40° North along the eastern Japanese coast. Comparison of run-up observations between consecutive points reveals differences of several tens of metres between points separated by only a couple of kilometres from each other. The spread of the distribution shown in figure 8 is typical of all tsunami events and underlines the need for tsunami forecast models targeted to specific coastal communities as opposed to a regional forecast.

Owing to the need for high-resolution grids for calculations of wave evolution in shallow water and inundation, and considering the time constraints associated with forecasting operations, it makes sense to focus computational resources on locations where the population is concentrated or where critical facilities are located.

For these reasons, the NOAA Center for Tsunami Research embarked, several years ago, on a project to develop 75 tsunami forecast models for at-risk US coastal communities in the Pacific and Atlantic Oceans. The models are integrated into a new tsunami forecasting software that incorporates all stages

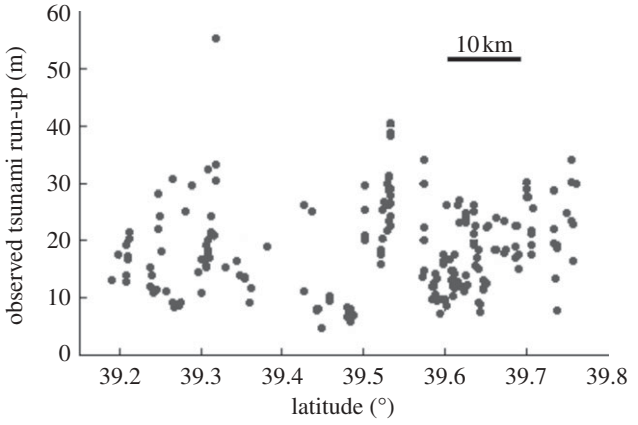

Figure 8. Run-up observations for the 11 March 2011 Japan tsunami along the eastern coast of Japan, showing a large amount of scattering between neighbouring coastal points ([37]; http://www.coastal.jp/tsunami2011/).

of the forecasting process described in this paper—generation, propagation and inundation—and is currently undergoing testing at the National Weather Service's tsunami warning centers.

The forecasting methodology presented in this section, based on state-of-the-art science and technology, has demonstrated its ability to generate accurate and valuable forecasts in real time during a number of events since 1993 [38]. Forecast results obtained by means of this methodology for a number of recent tsunami events can be accessed online at http://nctr.pmel.noaa.gov/database_devel.html. The forecast accuracy of this method is, of course, dependent on the density of the network of DART systems and on the magnitude of the event, with large events displaying a more favourable signal-to-noise ratio in the deep water, resulting in a more accurate inversion of the time series reported by the DART systems. The biggest challenge that this method faces is the reduction of the latency time, understood as the time elapsed between tsunami generation and the time when sufficient data have been reported by the first DART system, to issue a DART-based forecast. Densification of the DART network will help minimize this problem, as will an increase in sampling frequency of the sensors, so that the signature of seismic waves on water pressure at the sea floor can be resolved by the sensors and efficiently filtered out from the record. This will allow DART systems to be placed in closer proximity to earthquake epicentres, thereby reducing travel time of the wave to the sensor.

3. Mitigation of tsunami effects: lessons from Sumatra 2004, Chile 2010 and Japan 2011

The last 7 years have witnessed the destruction wreaked by three of the largest earthquakes and tsunamis ever recorded:

— In December 2004, an $M_w = 9.1$ earthquake and ensuing tsunami killed more than 200 000 people around the shores of the Indian Ocean.

— In February 2010, an $M_w = 8.8$ earthquake off the coast of Maule, Chile, generated an associated tsunami that caused inundation as far away as Japan.
— In March 2011, an $M_w = 9.0$ earthquake and tsunami on Honshu, Japan, caused thousands of casualties and has been considered as one of the worst nuclear disasters in history.

The unusual frequency and severity with which the world has been struck with the devastating effects of tsunamis in recent years, together with the abundance of audiovisual material of the disasters as they unfolded, have changed the perception of the general public with regard to the risk and destructive potential of tsunamis. It has also rekindled an interest by the different national and international authorities around the world to research methods and to implement policies designed to protect their populations and coastlines from tsunamis. In the USA, approximately 2 years after the Indian Ocean tsunami, the Tsunami Warning and Education Act was signed into public law. The intent of the law goes beyond protecting US population and property from future tsunamis—it recognizes the international nature of the hazard and it includes provisions for 'assistance to other nations to speed international efforts to establish regional tsunami warning systems in vulnerable areas worldwide, including the Indian Ocean' (Public Law 109-424-DEC. 20, 2006).

Similar efforts and legislation were passed in other countries vulnerable to tsunamis, mainly to enhance tsunami mitigation plans that might have been in place in Pacific Ocean nations prior to 2004, and to expand the efforts into other areas of the world, particularly, but not only, those bordering the Indian Ocean. These efforts are focused along three main lines of action: strengthening of tsunami forecasting and warning networks, increase in public awareness through education and outreach, and changes in public policy affecting zoning and location of critical facilities.

(*a*) *Strengthening of tsunami forecasting networks*

Section 2 has provided an overview of how current technology and scientific developments are being used to improve tsunami warning capabilities. In particular, we stressed that an effort is being made to move from a mere warning, understood as the notification that a tsunami may arrive at some shoreline, to a forecast or prediction of the event, understood as a description of the size of the expected waves, anticipated inundation areas, estimated strength of the currents, arrival time and decay rate. The idea is to be able to provide this information to local emergency managers, who may have to make fast decisions on the level of alert to be declared for a particular community. The main objective of these descriptive forecasts is to reduce the number of false alarms, which have occurred in the past with a large associated economic cost. There is another fundamental advantage to avoiding false alarms, which could be considered even more important than the first one. It is ensuring that the at-risk populations do not lose confidence in the accuracy of the information they receive. Loss of confidence due to previous false alarms may result in minimal or no reaction to the warning, which, in turn, undermines many of the preparedness efforts that may have been put in place.

Expansion of existing tsunami forecast networks and creation of others in places where they were non-existent prior to 2004 have received great emphasis since 2004. A good example of that is the number of DART systems deployed in the last 7 years, which has gone from eight systems prior to 2004 to the current network of 51 deployed in the Pacific, Indian and Atlantic Oceans (NDBC, http://www.ndbc.noaa.gov/dart.shtml).

(*b*) *Public outreach and education*

Regardless of whether a warning or forecast is issued, there is always some latency time between the generation of the tsunami and the dissemination of the message to the population. For some coastal areas in the near field of the earthquake, this latency time could delay the warning enough that the tsunami arrives before the warning is even issued. In these cases, the people need to be educated on how to interpret natural cues such as earthquake shaking or receding sea level as the warning for an impending tsunami and they need to have been previously instructed on how to proceed in such a situation. In other words, owing to the lack of time for warning and guidance from the authorities, the population needs to be able to act autonomously in the event of a tsunami. In order to make this possible, public education efforts, held periodically, are crucial in order to instruct the population on how to identify natural signs of an imminent tsunami, and how and where to evacuate if the need arises.

A clear example of how efficient in saving people's lives education can be is the anecdote of Tilly Smith, a 10 year old girl from Surrey, UK, who was on a beach in Phuket (Thailand), holidaying with her family during the Sumatra tsunami of 2004. She recognized the suddenly receding waterline and 'funny' behaviour of the ocean as the signs of an imminent tsunami, thanks to a geography class she had taken only a few weeks earlier. She expressed her concern to her parents, who alerted the hotel staff and other tourists. The tsunami struck only minutes later but nobody died on Mikhao Beach, where they were holidaying [39].

However, education without additional emergency and safety measures may not be enough. Another story, this time from the Chile 2010 tsunami, underlines the need for additional efforts to ensure that public education is successful in saving lives. The 2010 tsunami struck Chile at the end of the Austral summer. Every year the city of Constitución sees hundreds of its residents camp on Orrego Island, a flat island in the mouth of the Maule river, for a few days, to celebrate the end of the summer festival. The island is only a short 5 min boat-ride away from the main land. The local population has a long history of being exposed to tsunami hazard, and, in particular after the worldwide exposure of the Indian Ocean event, they were particularly aware of how to interpret the signs of a tsunami after a massive local earthquake. When the earthquake struck in the middle of the night, everybody on the island knew what was to come next, but, without bridges and only a couple of boats to evacuate the island, there was no possible escape for the hundreds of people who perished on the island (D. A. Marcelo Lagos 2010, personal communication). This clearly underlines the need for additional measures of preparedness beyond public education.

(*c*) *Emergency planning, inundation mapping and zoning laws*

From the last example in §3*b*, it becomes clear that the local authorities should be responsible not only for educating the public about tsunami hazard, but also for ensuring that the means are available for the at-risk population to proceed as they have been instructed during a tsunami event. For example, in the case of Orrego Island during the Chile 2010 tsunami, the local authorities should have prepared an evacuation plan for the island, perhaps in the form of vertical evacuation structures, which are man-made structures (several storeys high) designed to withstand an earthquake and ensuing tsunami, and designed to provide a safe haven for the population. Tentative design guidelines for such structures can be found in Yeh *et al.* [40].

In order for a coastal community to be able to design an effective tsunami evacuation plan, local authorities need to have an estimate of which areas of the community are likely to be inundated and will need to be evacuated, and which areas will be safe and can be used as gathering points by residents. They also need to be able to determine the safest way and fastest route to get the population to those areas, and to be able to disseminate this information among the population by means of evacuation maps prior to an event. These evacuation maps are designed with information provided by tsunami hazard assessment maps of the area. Tsunami hazard assessment maps reflect the results of numerical simulations of tsunami inundation in a specific community. These simulations are usually run at the highest available bathymetric and topographic resolution and are, typically, based on what is believed to be a worst credible tsunami-generating scenario for the area. In the aftermath of the Indian Ocean event, the National Tsunami Hazard Mitigation Program in the USA has encouraged development of hazard assessment and evacuation maps for at-risk communities at the state level [41]. However, the accuracy of these maps depends on the accuracy of our knowledge of the earthquake or tsunami source used in the study.

The earthquake and tsunami of Honshu, Japan, in 2011 provides a very good example of this limitation. The tsunami occurred in one of the areas of the world better prepared to cope with this type of disaster (recall that 'tsunami' is a Japanese word). Hazard assessment studies had been conducted, evacuation maps elaborated, sirens were in place to alert the population, and shelters or safe meeting areas had been identified in the event of a tsunami. Despite all of this planning, the loss of life was huge and the tsunami triggered one of the worst nuclear disasters in history. The answer to why this happened when so much planning ahead had taken place is simply that the earthquake (or 'source') generating the tsunami had been largely underestimated when conducting all these tsunami impact studies. People in Japan evacuated to what they believed to be safe havens only to be drowned by the water surge minutes later. The reactors in the Fukushima nuclear power plant overheated when the back-up power generators, which had been activated owing to a power failure from the earthquake, were then flooded, and sea walls that had been constructed for much smaller waves were overtopped by a massive wall of water 30 m high in some locations [37].

Japan 2011 is not an isolated case of source underestimation. If preparedness plans had been in place in the Indian Ocean prior to the Sumatra tsunami, they would have most probably also underestimated the source, since few seismologists

Figure 9. The Aneyoshi tablet's inscription reads: 'High dwellings are the peace and harmony of our descendants. Remember the calamity of the great tsunamis. Do not build any homes below this point' [43].

believed that an $M_w = 9.1$ earthquake could rupture in that area. The Sumatra event prompted the reassessment of the potential for a mega-thrust earthquake in other parts of the world [42]. Hence, the Cascadia subduction zone along the Pacific Northwest coast of the USA and Canada is now considered to have the potential to generate a significantly larger earthquake than previously estimated, and this concern is now being reflected in tsunami hazard assessment maps of the area.

In addition to evacuation maps, tsunami hazard assessments should be used to establish zoning laws. These laws can ensure that no critical facilities such as hospitals, fire stations, nuclear power plants, airports or densely populated residential areas are located in the tsunami inundation area. Or the laws can ensure that essential buildings in the inundation area satisfy building codes that make them tsunami-resistant, as proposed by Yeh *et al.* [40]. Tsunami-resistant structures located in the inundation zone can also serve as vertical evacuation structures for the population. Zoning restrictions along these lines had been passed from generation to generation in tsunami-prone communities, long before the advent of tsunami inundation models. Such was the case in the small village of Aneyoshi, Japan, where a centuries-old stone tablet, shown in figure 9, marked

the run-up limit of ancient tsunami events, indicating to village dwellers the lowest level at which they should build their homes in order to protect them from tsunamis.

The authors are grateful to the Fields Institute (in Toronto) for hosting a workshop in June 2011 on the Mathematics of Extreme Sea Waves, where the authors met and began this collaboration. We thank the organizers of that workshop: W. Craig, D. Henderson, E. Pelinovsky and C. Sulem. D. A. thanks Yong Wei and Liujuan Tang of the National Center for Tsunami Research for interesting discussions on tsunami generation, for their help in locating references and for creating figure 7. H. S. is grateful to the Erwin Schrödinger Institute (in Vienna), where he carried out some of this research. This work was supported in part by the Joint Institute for the Study of the Atmosphere and Ocean (JISAO) under NOAA Cooperative Agreement NA17RJ1232, Contribution no. 1884, and by the National Science Foundation, DMS-1107354.

Appendix A

(*a*) *Mathematical models of water waves*

In the simplest standard model for gravity-induced water waves on a free surface, the fluid is bounded below by a fixed, impermeable bed at $z=-d(x,y)$, and bounded above by a movable free surface at $z=\eta(x,y,t)$. The gravitational acceleration (g) is constant, gravity acts vertically downward and it is the only external force. The fluid is assumed to be homogeneous, incompressible and inviscid. Then Euler's equations in the fluid (i.e. for $-d(x,y)<z<\eta(x,y,t)$) are

$$\frac{\mathrm{D}u}{\mathrm{D}t}+\frac{1}{\rho}\frac{\partial p}{\partial x}=0, \tag{A 1a}$$

$$\frac{\mathrm{D}v}{\mathrm{D}t}+\frac{1}{\rho}\frac{\partial p}{\partial y}=0, \tag{A 1b}$$

$$\frac{\mathrm{D}w}{\mathrm{D}t}+\frac{1}{\rho}\frac{\partial p}{\partial z}=-g \tag{A 1c}$$

and

$$\frac{\partial u}{\partial x}+\frac{\partial v}{\partial y}+\frac{\partial w}{\partial z}=0, \tag{A 1d}$$

where $\{x,y\}$ are horizontal and $\{z\}$ is a vertical coordinate, $\boldsymbol{u}=(u,v,w)$ is the velocity vector, p is the pressure, ρ is the (constant) fluid density and the material derivative is

$$\frac{\mathrm{D}(\bullet)}{\mathrm{D}t}:=\frac{\partial(\bullet)}{\partial t}+u\frac{\partial(\bullet)}{\partial x}+v\frac{\partial(\bullet)}{\partial y}+w\frac{\partial(\bullet)}{\partial z}.$$

No fluid passes through the bottom so

$$\boldsymbol{u}\cdot\nabla(z+d)=0 \quad \text{on} \quad z+d(x,y)=0. \tag{A 1e}$$

On the free surface, at $z=\eta(x,y,t)$, the kinematic condition is

$$\frac{\partial\eta}{\partial t}+\boldsymbol{u}|_{\eta}\cdot\nabla\eta=w, \tag{A 1f}$$

while the dynamic condition prescribes the water pressure at the free surface as equal to the (constant) pressure above the surface,

$$p(x, y, z, t)|_{z=\eta} = p_0 = \text{const.} \tag{A 1g}$$

A special case of (A 1a–g) occurs if we also assume that the motion is irrotational. Then the fluid velocity is defined in terms of a velocity potential,

$$\boldsymbol{u} = \{u, v, w\} = \nabla\phi \quad \text{for} \quad -d(x, y) < z < \eta(x, y, t). \tag{A 2a}$$

Incompressibility and this representation combine to give

$$\nabla \cdot \boldsymbol{u} = \nabla^2\phi = 0 \quad \text{for} \quad -d(x, y) < z < \eta(x, y, t). \tag{A 2b}$$

The momentum equations, (A 1a–c), lead to Bernoulli's Law. Evaluating this condition on the free surface, and using (A 1g), leads to

$$\frac{\partial\phi}{\partial t} + \frac{1}{2}|\nabla\phi|^2 + g\eta + p_0 = 0 \quad \text{on} \quad z = \eta(x, y, t). \tag{A 2c}$$

The bottom boundary condition, written in terms of $\phi(x, y, z, t)$, becomes

$$\nabla\phi \cdot \nabla(z + d) = 0 \quad \text{on} \quad z = -d(x, y). \tag{A 2d}$$

(*b*) *Some approximate models*

The full equations of water waves are complicated, and so several approximate models have been derived, usually by taking various limits. The rest of this appendix reviews some approximate models.

- Linear theory appears in the limit: wave amplitude/depth $\to 0$.
- The shallow water equations appear in the limit: wavelength/depth $\to \infty$.
- The KdV equation and its cousins (Boussinesq, BBM) describe two-dimensional flows. All of them appear in the joint limit: wave amplitude/depth $\to 0$, wavelength/depth $\to \infty$. The Kadomtsev–Petviashvili (KP) equation generalizes KdV to three-dimensional flows.
- The Serre, Su–Gardner and Green–Naghdi equations are closely related to each other. They generalize the shallow water equations to allow for some wave dispersion.

Some of these models were first derived in the nineteenth century, but rigorous proof of their validity as approximations of the water wave equations has been much more recent. The recent work has depended on establishing the well-posedness of the water wave equations, pioneered by Wu [44,45]. See Alvarez-Samaniego & Lannes [46] and their references for more information about the mathematically rigorous validity of these models as approximations of the equations of (inviscid and irrotational) water waves.

- *Linear theory.* For waves of small amplitude on a fluid resting on a flat bottom (so $d = \text{const.}$), linearizing (A 2a–d) yields linear partial

differential equations with constant coefficients. These equations admit solutions in the form

$$\eta(x,y,t) = A\mathrm{e}^{\mathrm{i}kx+\mathrm{i}ly-\mathrm{i}\omega t} + (*),$$
$$\phi(x,y,z,t) = [B\mathrm{e}^{\mathrm{i}kx+\mathrm{i}ly-\mathrm{i}\omega t} + (*)]\frac{\cosh(\kappa(z+d))}{\cosh(\kappa d)}, \tag{A 3a}$$

where $\kappa^2 = k^2 + l^2$, and (*) denotes complex conjugate. This representation leads to the well-known dispersion relation for linearized water waves,

$$c^2 = \left(\frac{\omega}{\kappa}\right)^2 = gd\frac{\tanh(\kappa d)}{\kappa d}, \tag{A 3b}$$

which implies two important facts about gravity-driven water waves of small amplitude.

(i) $\mathrm{d}(c^2)/\mathrm{d}\kappa < 0$ for $0 < \kappa < \infty$. Thus, waves of small amplitude are *dispersive*, because waves with longer wavelengths travel faster than those with shorter wavelengths.

(ii) As $\kappa d \to 0$, $c^2 \to gd$. Thus, all long waves (i.e. with $\kappa d \ll 1$) of small amplitude travel with approximately the same speed: $\sqrt{gd}$. Wave dispersion becomes less important as $\kappa d \to 0$.

As asserted in §1*b*, individual fluid particles travel much more slowly than the tsunami in the open ocean. This claim can be confirmed easily in the linearized model. Linearizing (A 2*c*) leads to an approximate relation,

$$\frac{\partial\phi}{\partial t} + g\eta = 0 \quad \text{on} \quad z = 0.$$

For a two-dimensional, irrotational flow, the horizontal component of velocity of a plane wave is $\partial\phi/\partial x$; so, in the linearized problem, the horizontal velocity and the surface elevation are related by

$$u|_{z=0} = \frac{gk}{\omega}\eta. \tag{A 3c}$$

Thus, for a tsunami with a surface elevation of 1 m, propagating at $190\,\mathrm{m\,s^{-1}} \approx 650\,\mathrm{km\,h^{-1}}$, linear theory predicts that a fluid particle has a horizontal speed of $0.8\,\mathrm{km\,h^{-1}}$, which is less than $1\,\mathrm{km\,h^{-1}}$, as claimed. The analysis must be done differently for the *shallow water equations*, discussed next, but the outcome is about the same, because $\eta/d \ll 1$ in the open ocean. See Constantin [47] for an analysis of the trajectories of individual fluid particles in a periodic wave of permanent form, in an irrotational flow.

— *The shallow water equations*. Integrate (A 1*d*) in z, from the bottom of the fluid to the top, and use the boundary conditions in (A 1*e*,*f*) to obtain

$$\int_{-d}^{\eta}\left[\frac{\partial u}{\partial x} + \frac{\partial v}{\partial y}\right]\mathrm{d}z + \frac{\partial\eta}{\partial t} + \boldsymbol{u}|_{\eta}\cdot\nabla(\eta) - \boldsymbol{u}|_{-d}\cdot\nabla(-d) = 0.$$

Then integrate by parts to move the two derivatives outside the integral, and obtain

$$\frac{\partial \eta}{\partial t} + \frac{\partial}{\partial x}\int_{-d}^{\eta} [u]\mathrm{d}z + \frac{\partial}{\partial y}\int_{-d}^{\eta} [v]\mathrm{d}z = 0. \tag{A 4a}$$

This statement, of conservation of total mass of the fluid, is exact. The next step requires approximations. Suppose that the vertical motion of the fluid is small. For it to remain small, vertical acceleration must also remain small. Then the vertical acceleration ($\mathrm{D}w/\mathrm{D}t$) is negligible in (A 1c), which becomes an ordinary differential equation for $p(x, y, z, t)$. Integrate it, and use (A 1g) to obtain the required constant of integration. The result is that the pressure must be hydrostatic in the fluid,

$$p(x, y, z, t) = g\rho \cdot \{\eta(x, y, t) - z\} + p_0. \tag{A 4b}$$

Substitute this into (A 1a,b), and neglect $w\partial_z(\bullet)$ in $\mathrm{D}(\cdot)/\mathrm{D}t$ (because w is assumed small) to obtain

$$\frac{\partial u}{\partial t} + u\frac{\partial u}{\partial x} + v\frac{\partial u}{\partial y} + g\frac{\partial \eta}{\partial x} = 0 \tag{A 4c}$$

and

$$\frac{\partial v}{\partial t} + u\frac{\partial v}{\partial x} + v\frac{\partial v}{\partial y} + g\frac{\partial \eta}{\partial y} = 0. \tag{A 4d}$$

If (u, v) initially have no z-dependence, then they maintain that property according to (A 4c,d), so (A 4a) can be simplified to

$$\frac{\partial \eta}{\partial t} + \frac{\partial}{\partial x}\{(\eta + d)u\} + \frac{\partial}{\partial y}\{(\eta + d)v\} = 0. \tag{A 4e}$$

Equations (A 4c–e) are the *shallow water equations*, originally due to Venant [48]. They are basic ingredients in the operational models discussed in §2. Here are some properties of these equations.

(i) The equations are hyperbolic; they involve only first derivatives of the unknowns.

(ii) The speed of propagation of any disturbance is $\sqrt{g(\eta + d)}$; this is a nonlinear generalization of the speed, $\sqrt{gd}$, given by the linearized theory.

(iii) All infinitesimal disturbances travel with the same speed at any fixed d, so the equations are *non-dispersive*. Any dispersion observed in actual water waves is not described by these equations.

(iv) The equations are nonlinear and hyperbolic, so solutions of the equations can 'break': i.e. initially smooth solutions can become discontinuous in finite time. Methods to continue the solution after the point of wave-breaking are not unique.

— *KdV-type models*. The two approximate models discussed so far allow: (i) for waves of any wavelength, but only infinitesimal amplitudes (see (A 3)) or (ii) for waves of any amplitude, but then only for very long wavelengths (see (A 4c–e)). Another family of approximate models aims

to bridge this divide, by allowing small but finite amplitudes and long, but not infinitely long, wavelengths. This family includes equations named after Boussinesq [49], Korteweg & de Vries [4], Kadomtsev & Petviashvili [50] and Benjamin–Bona–Mahony [51]. For simplicity, we outline only the derivations of KdV and/or KP here, and we consider only the case of a flat bottom ($d = \text{const.}$). More details can be found in Ablowitz & Segur [5], Johnson [52] or elsewhere.

The KdV and KP equations each approximate (A 2*a*–*d*) in specific limits, when length scales are ordered in a specific way. One needs:

(i) wave amplitudes much smaller than the fluid depth;

(ii) fluid depth much smaller than the wavelength in the direction of propagation;

(iii) wavelength in direction of propagation much smaller than transverse wavelength (so all waves are travelling in nearly the same direction)—one can get either KdV or KP, depending on the strength of this transverse variation;

(iv) all three small effects of comparable size.

Then one introduces a formal small parameter ($\varepsilon \ll 1$) to formalize this ordering, scales the variables in (A 2*a*–*d*) in a way consistent with the ordering and derives approximate equations, order by order, in ε. At leading order, the waves have infinitesimal amplitude, infinitely long wavelengths and the fluid motion is exactly one dimension. Hence, as (A 4) suggests, the waves must satisfy the linear wave equation in one dimension, (1.1), with solution

$$\eta(x, y, t; \varepsilon) = \varepsilon[F(x - \sqrt{gd}\cdot t) + G(x + \sqrt{gd}\cdot t)] + O(\varepsilon^2). \qquad \text{(A 5}a\text{)}$$

At this order of approximation, all waves travel with the same speed, $\sqrt{gd}$. The initial data determine $F(\chi)$ and $G(\zeta)$, each of which then travels as a wave of permanent form. This description is approximately correct for short times. But the small effects that are unimportant for short times can build up to have a cumulative effect over longer times. One can see this by introducing a slow time scale (either $\tau = \varepsilon t$ or $\tau = \varepsilon x/\sqrt{gd}$), defining $\chi = x - \sqrt{gd}\cdot t$, allowing $F = F(\chi, \tau) + \mathrm{O}(\varepsilon)$, and following the F-wave as it propagates. By standard asymptotic procedures, if there is no y-dependence, then one finds that $F(\chi, \tau)$ satisfies a KdV equation equivalent to

$$\frac{\partial F}{\partial \tau} + F\frac{\partial F}{\partial \chi} + \frac{\partial^3 F}{\partial \chi^3} = 0, \qquad \text{(A 5}b\text{)}$$

and that $G(\zeta, \tau)$ satisfies another KdV equation. The last two terms in (A 5*b*) determine how F (or G) evolves on a long time scale, in response to small but cumulative nonlinear effects (through $F(\partial F/\partial \chi)$) and in response to small but cumulative wave dispersion (through $\partial^3 F/\partial \chi^3$). The coefficients of these two terms are usually not unity, but they can usually be scaled to unity by suitably redefining F and χ. If there is y-dependence

of the right magnitude, then set $\psi = \varepsilon y$, $F = F(\chi, \psi, \tau) + O(\varepsilon)$, and find that F satisfies not a KdV equation but a KP equation,

$$\frac{\partial}{\partial \chi}\left[\frac{\partial F}{\partial \tau} + F\frac{\partial F}{\partial \chi} + \frac{\partial^3 F}{\partial \chi^3}\right] \pm \frac{\partial^2 F}{\partial \psi^2} = 0. \tag{A 5c}$$

As in (A 5*b*), the coefficients in (A 5*c*) are typically not unity, but they can be rescaled.

One advantage of a KdV model (or other members of this family) over either the linearized model in (A 3) or the shallow water model in (A 4*c*–*e*) is that the KdV model allows for both nonlinearity and dispersion, while (A 3) and (A 4*c*–*e*) each allow for only one of these effects. But one pays for this extra flexibility in two ways:

(a) both nonlinearity and dispersion must be weak in order to obtain a KdV-like equation; and

(b) these small effects only influence wave dynamics on a longer time scale.

On a shorter time scale, an equation like those in (1.1) or (1.2) gives a suitable approximate description.

Now we can finally give meaning to the concepts of 'long time' and 'short time', used in §1. Tsunamis are usually long waves of small amplitude. The linear wave equation, (1.2), describes the propagation of these waves until (1.2) becomes an invalid approximation, because either nonlinear effects or wave dispersion becomes important. So 'short time' is the time before either nonlinearity or dispersion has become important, and 'long time' is when one or both of these effects is/are dynamically important. Here are some criteria to identify this change-over:

(i) Long waves propagate with speed $\sqrt{gd}$ according to the linear wave equation, but with speed $\sqrt{g(\eta + d)}$ according to the (nonlinear) shallow water equations so $\sqrt{gd} \cdot (|\eta|/2d)$ approximates the difference in the two speeds. If L is a typical length scale in the initial data, then $(L/\sqrt{gd})$ is a typical 'short' time scale, and $(L/\sqrt{gd}) \cdot (d/|\eta|)$ is a 'long' time scale.

(ii) Waves with wavenumber κ propagate with speed $\sqrt{g\kappa \cdot \tanh(\kappa d)}$ according to linear theory, (A 3*b*), while the linearized wavefront propagates with speed $\sqrt{gd}$. For $\kappa = 2\pi/L$, where L is a typical initial length scale, $(L/\sqrt{gd})(L/d)^2$ is a time by which the wave energy at this wavelength has fallen behind the wavefront by a distance comparable to L, so $(L/\sqrt{gd})(L/d)^2$ is another 'long' time scale.

(iii) The shallow water equations are hyperbolic, so one can solve them by the method of characteristics. The shallow water model breaks down when characteristics of the same family cross. This certainly marks the end of the 'short' time scale, not because wave amplitudes have become large, but because waves with short wavelength have built up near the point where the characteristics cross. This process is evident in figures 2 and 3.

(iv) Generally, 'short time' is the time before any of these effects occurs, and 'long time' begins when the first of them becomes significant.

— *The Serre/Su–Gardner/Green–Naghdi equations.* The shallow water equations, (A 4*c–e*), were generalized in essentially the same way by Serre [53,54], Su & Gardner [55] and Green & Naghdi [56]. Their methods were different, so it was not immediately obvious that their approximate models were nearly identical.

For a two-dimensional flow (i.e. with $v=0$, $\partial(\bullet)/\partial y=0$) on a horizontal bed (so $d=\text{const.}$), define

$$h(x,t)=\eta(x,t)+d.$$

Then the two-dimensional shallow water equations, (A 4*c*,*e*), become

$$\frac{\partial u}{\partial t}+u\frac{\partial u}{\partial x}+g\frac{\partial h}{\partial x}=0 \quad \text{and} \quad \frac{\partial h}{\partial t}+\frac{\partial}{\partial x}(h\cdot u)=0.$$

The Serre/Su–Gardner/Green–Naghdi equations add a correction to these equations, obtained by approximating the vertical momentum equation less drastically than with the hydrostatic approximation,

$$\frac{\partial u}{\partial t}+u\frac{\partial u}{\partial x}+g\frac{\partial h}{\partial x}=\frac{1}{3h}\frac{\partial}{\partial x}\left[h^3\left(\frac{\partial^2 u}{\partial x\partial t}+u\frac{\partial^2 u}{\partial x^2}-\left(\frac{\partial u}{\partial x}\right)^2\right)\right], \tag{A 6a}$$

$$\frac{\partial h}{\partial t}+\frac{\partial}{\partial x}(h\cdot u)=0. \tag{A 6b}$$

See El *et al.* [57], Alvarez-Samaniego & Lannes [46], Dias & Milewski [58], Carter & Cienfuegos [59] and their references for analysis of these equations.

References

1 Gusiakov, V. K. 2009 Tsunami history: recorded. In *The sea*, vol. 15 (eds E. R. Bernard & A. R. Robinson). Cambridge, MA: Harvard University Press.

2 Geist, E. L., Titov, V. V., Arcas, D., Pollitz, F. F. & Bilek, S. L. 2007 Implications of the 26 December 2004 Sumatra–Andaman Earthquake on tsunami forecast and assessment models for great subduction-zone earthquakes. *Bull. Seis.* **97**, S249–S270. (doi:10.1785/0120050619, S249–S270)

3 Powers, D. L. 1972 *Boundary value problems.* New York, NY: Academic Press.

4 Korteweg, J. D. & de Vries, G. 1895 On the change of form of long waves advancing in a rectangular canal, and on a new type of long stationary wave. *Phil. Mag. Ser. 5* **39**, 422–443. (doi:10.1080/14786449508620739)

5 Ablowitz, M. J. & Segur, H. 1981 *Solitons and the inverse scattering transform.* Philadelphia, PA: SIAM.

6 Pelinovsky, E. N. 1982 *Nonlinear dynamics of tsunami* [in Russian]. Nizhny Novgorod, Russia: Gorky Institute of Applied Physics Press.

7 Craig, W. 2006 Surface water waves and tsunamis. *J. Dyn. Diff. Equ.* **18**, 525–549. (doi:10.1007/s10884-006-9031-4)

8 Segur, H. 2007 Waves in shallow water, with emphasis on the tsunami of 2004. In *Tsunamis and nonlinear waves* (ed. A. Kundu), pp. 3–29. New York, NY: Springer.

9 Constantin, A. & Johnson, R. S. 2008 Propagation of very long water waves, with vorticity, over variable depth, with application to tsunamis. *Fluid Dyn. Res.* **40**, 175–211. (doi:10.1016/j.fluiddyn.2007.06004)

10 Grue, J., Pelinovsky, E. N., Fructus, D., Talipova, T. & Kharif, C. 2008 Formation of undular bores and solitary waves in the Strait of Malacca caused by the 26 December 2004 Indian Ocean tsunami. *J. Geophys. Res.* **113**, C05008. (doi:10.1029/2007JC004343)
11 Madsen, P. A., Fuhrman, D. R. & Schäffer, H. A. 2008 On the solitary wave paradigm for tsunamis. *J. Geophys. Res.* **113**, C12012. (doi:10.1029/2008JC004932).
12 Lax, P. D. 1973 *Hyperbolic systems of conservation laws and the mathematical theory of shock waves*. Philadelphia, PA: SIAM.
13 Gurevich, A., Anderson, D. & Wilhelmsson, H. 1979 Ion acceleration in an expanding rarified plasma with non-Maxwellian electrons. *Phys. Rev. Lett.* **42**, 769–772. (doi:10.1103/PhysRevLett.42.769)
14 Hoefer, M. A., Ablowitz, M. J., Coddington, I., Cornell, E. A., Engels, P. & Schweikhard, V. 2006 Dispersive and classical shock waves in Bose–Einstein condensates and gas dynamics. *Phys. Rev. A* **74**, 023623. (doi:10.1103/PhysRevA.74.023623)
15 Hammack, J. L. 1973 Note on tsunamis—their generation and propagation in an ocean of uniform depth. *J. Fluid Mech.* **60**, 769–799. (doi:10.1017/S0022112073000479)
16 Hammack, J. L. & Segur, H. 1974 The Korteweg–deVries equation and water waves. II. Comparison with experiments. *J. Fluid Mech.* **65**, 289–314. (doi:10.1017/S002211207400139X)
17 Hammack, J. L. & Segur, H. 1978 The Korteweg–deVries equation and water waves. III. Oscillatory waves. *J. Fluid Mech.* **84**, 337–358. (doi:10.1017/S0022112078000208)
18 Shuto, N. 1991 Numerical simulations of tsunamis: its present and near future. In *Tsunami hazards* (ed. E. Bernard), pp. 171–191. Dordrecht, The Netherlands: Kluwer Academic Publishers.
19 Burwell, D., Tolkova, E. & Chawla, A. 2007 Diffusion and dispersion characterization of a numerical tsunami model. *Ocean Model.* **19**, 10–30. (doi:10.1016/j.ocemod.2007.05.003)
20 Rao, N. P. 2007 Characterization of potential tsunamigenic earthquake source zones in the Indian Ocean. In *Tsunamis and nonlinear waves* (ed. A. Kundu), pp. 285–312. New York, NY: Springer.
21 Gonzalez, F. I., Bernard, E. N., Meinig, C., Eble, M., Mofjeld, H. O. & Stalin, S. 2005 The NTHMP tsunameter network. *Nat. Hazards* **35**, 25–39A. (doi:10.1007/s11069-004-2402-4)
22 Spillane, M. C., Gica, E., Titov, V. V. & Mofjeld, H. O. 2008 Tsunameter network design for the U.S. DART® arrays in the Pacific and Atlantic Oceans. NOAA Tech. Memo. OAR PMEL-143. Seattle, WA: Pacific Marine Environmental Laboratory.
23 Todorovska, M. & Triffunac, M. D. 2001 Generation of tsunamis by a slowly spreading uplift of the sea floor. *Soil Dyn. Earthq. Eng.* **21**, 151–167. (doi:10.1016/S0267-7261(00)00096-8)
24 Heidarzadeh, M. 2011 Major tsunami risk from splay faulting. In *The tsunami threat: research and technology* (ed. N.-A. Mörner), pp. 67–80. Rijeka, Croatia: InTech.
25 Smith, W. H. F., Scharroo, R., Titov, V. V., Arcas, D. & Arbic, B. K. 2005 Satellite altimeters measure tsunami. *Oceanography* **18**, 11–13.
26 Hammond, W. C., Brooks, B. A., Bürgmann, R., Heaton, T., Jackson, M. & Lowry, A. R. 2011 Scientific value of real-time global positioning system data. *Eos Trans. Am. Geophys. Union* **92**, 125–132. (doi:10.1029/2011EO150001)
27 Arcas, D. & Wei, Y. 2011 Evaluation of velocity-related approximations in the non-linear shallow water equations for the Kuril Islands, 2006 tsunami event at Honolulu, Hawaii. *Geophys. Res. Lett.* **38**, L12608. (doi:10.1029/2011GL047083).
28 Tadepalli, S. & Synolakis, C. E. 1994 The run-up of N-waves over sloping beaches. *Proc. R. Soc. Lond. A* **445**, 99–112. (doi:10.1098/rspa.1994.0050)
29 Tadepalli, S. & Synolakis, C. E. 1996 Model for the leading waves of tsunamis. *Phys. Rev. Lett.* **77**, 2141–2144. (doi:10.1103/PhysRevLett.77.2141)
30 Satake, K. 2007 Tsunamis. In *Treatise on geophysics*, vol. 4 (ed. G. Schubert), pp. 483–511. Amsterdam, The Netherlands: Elsevier.
31 Gica, E., Spillane, M., Titov, V. V., Chamberlin, C. & Newman, J. C. 2008 Development of the forecast propagation database for NOAA's Short-term Inundation Forecast for Tsunamis (SIFT). NOAA Tech. Memo. OAR PMEL-139. Seattle, WA: Pacific Marine Environmental Laboratory.

32 Okada, Y. 1985 Surface deformation due to shear and tensile faults in a half-space. *Bull. Seismol. Soc. Am.* **75**, 1135–1154.
33 Percival, D. B., Denbo, D. W., Eble, M. C., Gica, E., Mofjeld, H. O., Spillane, M. C., Tang, L. & Titov, V. V. 2010 Extraction of tsunami source coefficients via inversion of DART® buoy data. *Nat. Hazards.* **58**, 567–590. (doi:10.1007/s11069-010-9688-1)
34 Arcas, D. & Wei, Y. 2011 Evaluation of velocity-related approximations in the non-linear shallow water equations for the Kuril Islands, 2006 tsunami event at Honolulu, Hawaii. *Geophys. Res. Lett.* **28**, L12608. (doi:10.1029/2011GL047083)
35 Tang, L., Titov, V. V. & Chamberlin, C. D. 2009 Development, testing, and applications of site-specific tsunami inundation models for real-time forecasting. *J. Geophys. Res.* **114**, C12025. (doi:10.1029/2009JC005476)
36 Intergovernmental Oceanographic Commission. 1998 *Post-tsunami survey field guide*. Manuals and Guides no. 37. Paris, France: UNESCO. See http://ioc3.unesco.org/itic/files/MG037.pdf.
37 The 2011 Tohoku Earthquake Tsunami Joint Survey Group. 2011 *The 2011 Tohoku earthquake tsunami information*. See http://www.coastal.jp/tsunami2011.
38 Wei, Y., Bernard, E., Tang, L., Weiss, R., Titov, V., Moore, C., Spillane, M., Hopkins, M. & Kânoğlu, U. 2008 Real-time experimental forecast of the Peruvian tsunami of August 2007 for U.S. coastlines. *Geophys. Res. Lett.* **35**, L04609. (doi:10.1029/2007GL032250)
39 Anon. 2005. Girl, 10, used geography lesson to save lives. *Daily Telegraph*, 1 January 2005. See http://www.telegraph.co.uk/news/1480192/Girl-10-used-geography-lesson-to-save-lives.html
40 Yeh, H., Robertson, I. & Preuss, J. 2005 Development of design guidelines for structures that serve as tsunami vertical evacuation sites. Open File report, 2005-4. Washington Division of Geology and Earth Resources. See http://www.dnr.wa.gov/Publications/ger_ofr20054_tsunami_evac_site_design_guidelines.zip.
41 Committee on the Review of the Tsunami Warning and Forecast System and Overview of the Nation's Tsunami Preparedness. National Research Council of the National Academies. 2011 *Tsunami warning and preparedness: an assessment of the U.S. tsunami program and the nation's preparedness efforts*. Washington, DC: The National Academies Press.
42 Stein, S. & Okal, E. A. 2007 Ultra-long period seismic study of the December 2004 Indian Ocean earthquake and implications for regional tectonics and the subduction process. *Bull. Seismol. Soc. Am.* **97**, S279–S295. (doi:10.1785/0120050617)
43 Alabaster, J. 2011 Tsunami-hit towns forgot warnings from ancestors. See http://www.newsvine.com/_news/2011/04/06/6418935-tsunami-hit-towns-forgot-warnings-from-ancestors.
44 Wu, S. 1997 Well-posedness in Sobolev spaces of the full water wave problem in 2-D. *Invent. Math.* **130**, 39–72. (doi:10.1007/s002220050177)
45 Wu, S. 1999 Well-posedness in Sobolev spaces of the full water wave problem in 3-D. *J. Am. Math Soc.* **12**, 445–595. (doi:10.1090/S0894-0347-99-00290-8)
46 Alvarez-Samaniego, B. & Lannes, D. 2009 Large-time existence for 3D water waves and asymptotics. *Invent. Math.* **171**, 165–186.
47 Constantin, A. 2006 The trajectories of particles in Stokes waves. *Invent. Math.* **166**, 523–535. (doi:10.1007/s00222-006-0002-5)
48 Venant St, A. J. C. B. 1871 Théorie du mouvement non-permanent des eaux avec applications aux crues des rivieres et a l'introduction des marées dans leur lit. *Comptes Rendues* **73**, 147–154.
49 Boussinesq, J. 1872 Theorie des ondes et de remous qui se propagent…. *J. Math. Pures Appl. Ser. 2* **17**, 55–108.
50 Kadomtsev, B. B. & Petviashvili, V. I. 1970 On the stability of solitary waves in weakly dispersive media. *Sov. Phys. Doklady* **15**, 539–541.
51 Benjamin, T. B., Bona, J. L. & Mahony, J. J. 1972 Model equations for long waves in nonlinear dispersive systems. *Phil. Trans. R. Soc. Lond. A* **272**, 47–78. (doi:10.1098/rsta.1972.0032)
52 Johnson, R. S. 1997 *A modern introduction to the mathematical theory of water waves*. Cambridge, UK: Cambridge University Press.
53 Serre, F. 1953 Contribution á l'étude des écoulements permanents et variables dans les caneux. *Houille Blanche* **8**, 374–388. (doi:10.1051/lhb/1953034)
54 Serre, F. 1953 Contribution á l'étude des écoulements permanents et variables dans les caneux (FIN). *Houille Blanche* **8**, 830–872. (doi:10.1051/lhb/1953058)

55 Su, C. H. & Gardner, C. S. 1969 KdV equation and generalizations. III. Derivation of Korteweg–de Vries equation and Burgers equation. *J. Math. Phys.* **10**, 536–539. (doi:10.1063/1.1664873)
56 Green, E. A. & Naghdi, P. M. 1976 A derivation of equations for wave propagation in water of variable depth. *J. Fluid Mech.* **78**, 237–246. (doi:10.1017/S0022112076002425)
57 El, G. A., Grimshaw, R. H. J. & Smyth, N. F. 2006 Unsteady undular bores in fully nonlinear shallow-water theory. *Phys. Fluids* **18**, 027104. (doi:10.1063/1.2175152)
58 Dias, F. & Milewski, P. 2010 On the fully-nonlinear shallow-water generalized Serre equations. *Phys. Lett. A* **374**, 1049–1053. (doi:10.1016/j.physleta.2009.12.043)
59 Carter, J. D. & Cienfuegos, R. 2011 The kinematics and stability of solitary and cnoidal wave solutions of the Serre equations. *Euro. J. Mech. B: Fluids* **30**, 259–268. (doi:10.1016/j.euromechflu.2010.12.002)